Chapter 4

Polarization Analysis of Millisecond Pulsars

4.1 Pulsar Geometry

The polarization data presented in Chapter 3 indicate that the polarization position angle (PPA) curve remains approximately the same for all radio frequencies. The rotating vector model discussed in Section 1.4 can therefore, in principle, be used in conjunction with the PPA results to determine the geometry for these millisecond pulsars. This is not straightforward, due to the presence of orthogonal modes, the limited longitude range of the PPA data, and the fact that the effect of magnetic inclination α on the PPA curve can be quite subtle. Investigation of the evolution of the intensity profile with frequency sometimes allows the pulse components to be classified as core or cone, which can help to constrain the emission geometry.

The intrinsic distribution of magnetic inclinations α is uniform for slow pulsars, as noted in Section 1.4. This may not necessarily be true for millisecond pulsars. Observations of binary pulsars offer other clues to the geometry. The spin and orbit angular momentum axes are expected to be aligned, due to the evolutionary spin-up of these objects via mass accretion. The mass function

$$f(M_c) = \frac{(M_c \sin i)^3}{(M_{NS} + M_c)^2} = \frac{4\pi^2 (a \sin i)^3}{G P_{orb}^2} \tag{4.1}$$

relates the companion mass M_c to the orbital period P_{orb} and projected semi-major axis $a \sin i$, where the inclination i of the orbit is unknown. A calculation of the minimum companion mass compatible with the observations is therefore possible. Backer (1998) discussed the population of rapidly rotating pulsars with Helium white dwarf companions, and concluded that the observed distribution of minimum companion masses required non-random inclinations. One possible explanation is that the magnetic and spin axes are preferentially orthogonal, so we see only binary systems with

$i = \alpha \sim 90°$. Chen & Ruderman (1993a) predict an unusual magnetic field topology for these objects that results in a preference for inclinations of 90°. If the pulsars in this class are all nearly orthogonal, then it is possible that this geometry extends to other millisecond pulsars as well. This hypothesis would predict that almost all millisecond pulsars would exhibit a pulse-interpulse morphology, if radio emission occurs within the broad beam at *both* magnetic poles. Several objects do not have interpulse components in their pulse profiles.

A theoretical relation between white dwarf mass and orbital period can also be used to constrain values of α. Rappaport *et al.* (1995) discuss the theoretical evolution of binary stars leading to pulsar systems with low-mass white dwarf companions in nearly circular orbits, and orbital periods in excess of one day. These evolutionary calculations lead to the expectation that the orbital period and white dwarf mass are related. If their model is correct, then this relation can be combined with the mass function to give the inclination $i = \alpha$ of the system, again with the assumption that the orbital and spin angular momentum axes are aligned. This value of α can then be used to constrain the rotating vector model fits to the PPA data. In general, the relation yields $i = \alpha \neq 90°$.

4.2   PPA Fits

The multifrequency polarization position angle data presented in Chapter 3 were fit to a rotating vector model (equation 1.4) at each individual radio frequency. The fit included the geometric parameters α and β, as well as pulse longitude and PPA offsets. Any apparent orthogonal mode transitions were removed prior to the fit. In order to reduce the sensitivity of the fit to the region in pulse phase immediately surrounding an orthogonal mode transition, the PPAs were weighted by the SNR of the linear polarization, which decreases during an orthogonal mode transition. This also prevented the fit from becoming biased by the random PPAs between pulse components. For fixed α, the other parameters were varied until a satisfactory fit was obtained. Various values of α were used, and the results compared. In some cases, the location of the center of symmetry for the rotating vector model was poorly constrained, and was held fixed at a particular pulse longitude. Values of magnetic inclination $90° < \alpha < 180°$ and impact parameter β relative to the rotation axis are equivalent to a measurement of $\alpha' = 180° - \alpha$, $\beta' = -\beta$ relative to the opposite rotation axis. For comparison to the predictions based on orbital inclinations, α' should be used. The PPA data are measured counter-clockwise from north on the plane of the sky, contrary to the suggestion of Arzoumanian *et al.* (1996). This failure to flip the sign of the PPA data so that they are measured clockwise changes none of

the geometrical conclusions, but simply moves the magnetic axis from the proximity of one rotational pole to the other.

The intensity data for each pulsar are presented once again, this time in the form of a log-polar diagram, for the purpose of investigating the structure of the emission beam. In these diagrams, first used by Hankins & Fowler (1986), the relative intensity is plotted (on a logarithmic scale) in polar coordinates, using the pulse phase as the angle. The geometrical radiation pattern of the pulsar is immediately apparent. An example is Figure 4.1. Dotted circles represent the level of maximum emission, 10% emission, and (when shown) 1% emission. The radiation pattern rotates clockwise with respect to a fixed observer to reproduce the polarization profile vs. pulse longitude plots displayed in Chapter 3 (cf. Figure 3.2). The PPA data and accompanying fits are plotted on an enlarged scale for each pulsar, as is shown for PSR J0613−0200 in Figure 4.2. The smoothed polarization profile is located at the top of each plot for reference purposes. The polarization position angle is duplicated and plotted over the range −180 to 180° for clarity. Rotating vector model fits are represented by smooth lines through the data. A legend accompanies each plot.

Table 4.1 lists the derived fit parameters α, β and the maximum slope $(d\psi/d\phi)_{max}$ for each pulsar. Any temporal variations in the intensity or polarization profile are also noted here.

Pulsar Geometries and Moding Behaviour

Source	α (°)	β (°)	$\left(\dfrac{d\psi}{d\phi}\right)_{max}$ (°/°)	$\left(\dfrac{d\psi}{d\phi}\right)_{xil}$ (°/°)	Profile Variation	Polarization Variation	Comments
				Multifrequency Data			
J0613−0200	−	~ −10	-2.4	−		p	
J1012+5307	40	11	3.5	-2.7		y	
J1022+1001	60	6	9	6	y	y	well-defined PPA
B1620−26	−	−	2.6	-1.5		p	
J1713+0747	105	-18	-3.	-1.7		y	
J1730−2304	−	−	-1.	2.2	x	x	
B1821−24	50	40	1.2	−	y	y	outer-gap emission?
B1937+21	−	−	-.8	−			Crab-like
J2145−0750	90	16	3.6	-.65	y	y	complex PPA
				1410-MHz Data			
J0751+1807	−	−	−	−		x	
J1518+4904	−	−	−	−		p	
J1640+2224	−	−	−	−		p	
J1643−1224	−	−	−	−		p	
				Xilouris et al. (1998)			
B1855+09	−	−	−	−		x	
B1953+29	−	−	−	−	?	x	

Table 4.1: Information on the pulsar's geometry and moding behaviour are summarized for our multifrequency observations. The magnetic inclination α and impact parameter β given in columns 2 and 3 are given whenever our fitting procedure yielded a preferred result. They are not necessarily well-determined. The maximum slopes $(d\psi/d\phi)_{max}$ tabulated in column 4 are derived from these and other fits, or estimated from the data when a fit was unavailable. The values quoted by Xilouris *et al.* (1998) are quoted in column 5 for comparison. The main thing to note is the fact that the slopes are relatively flat for all objects, even when the detailed models are different. Columns 6 and 7 describe the presence of profile and polarization variations, respectively: y-seen in our data, p-possibly seen in comparison with data of Xilouris *et al.* (1998), x-Xilouris *et al.* (1998) report variations. These are also reported for the objects for which we have only 1410-MHz observations. Two other objects exhibiting temporal variations in the dataset of Xilouris *et al.* (1998) are also included.
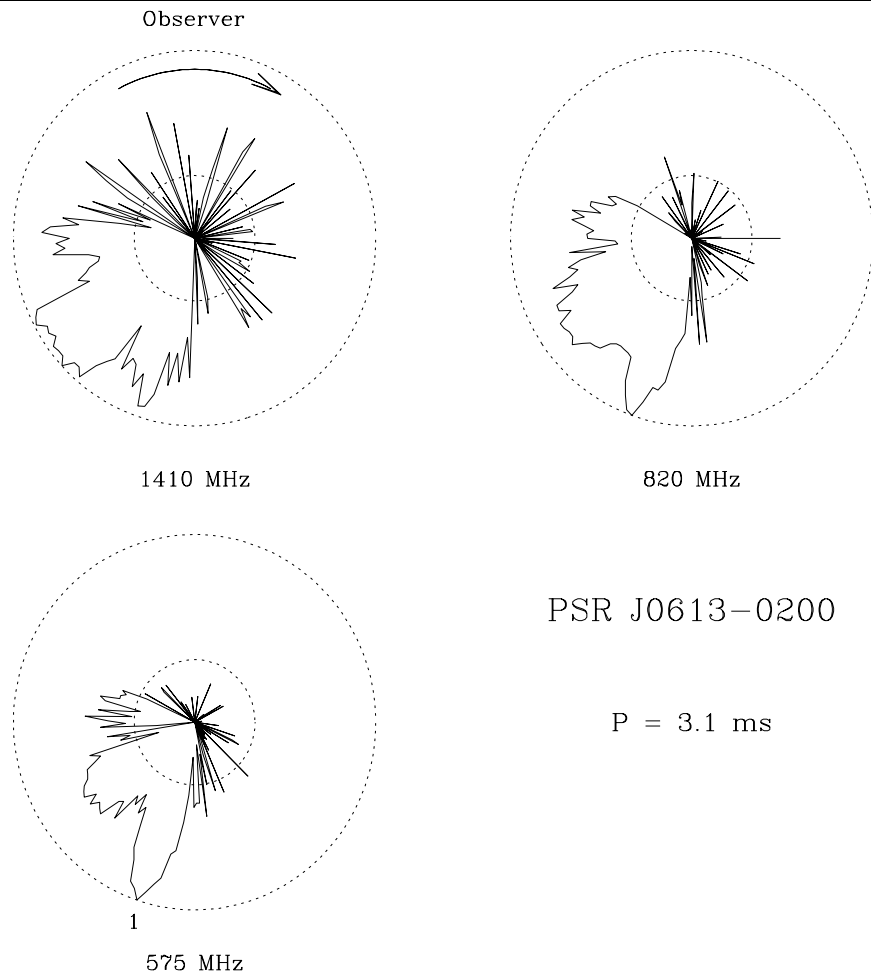
Fig. 4.1.— The relative intensity of PSR J0613−0200 is presented at each radio frequency in a log-polar plot. The intensity, on a logarithmic scale, is presented (solid lines) in polar coordinates, using pulse phase as the angle. The dotted circles represent the levels of maximum emission and 10% of this value. Component 1 in the fits of Chapter 3 is identified in the 575-MHz data.

4.2.1 PSR J0613−0200

This 3.06 millisecond pulsar has a binary companion with mass $0.13 M_\odot / \sin i$ (Lorimer *et al.* 1995a) in a 28.8 hour orbit. This object is one of the pulsars which Backer (1998) considered in concluding that the inclinations were not random. Equation 4.1 predicts an inclination of 66°, although the orbital period is at the lower end of the range for which their model is valid, and the relationship is more uncertain there (Rappaport *et al.* 1995).

Based on the spectral and polarization behaviour of the components, we would expect the trailing sharp feature (component 1 in Figure 4.1) to be identified as a core component. The substantial offset of this component from the symmetry center of the pulse is not at all in line with this interpretation.
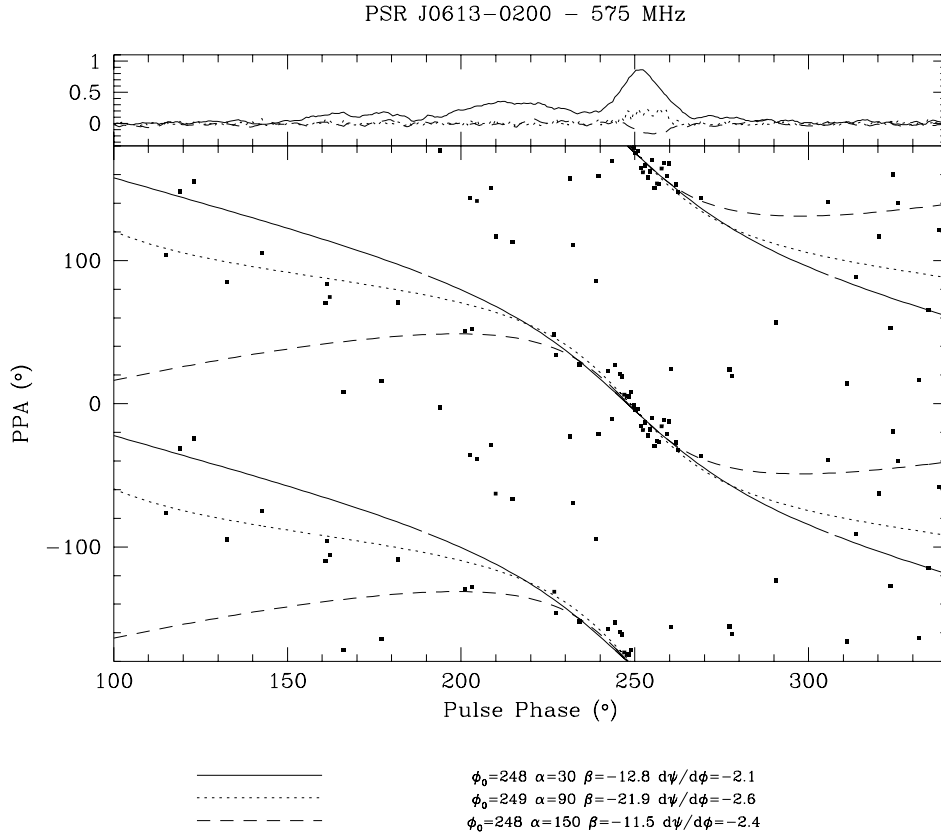
PSR J0613−0200 − 575 MHz

Fig. 4.2.— Rotating vector models are fit to the PPA data of PSR J0613−0200 at 575 MHz. The data (filled squares) are plotted against pulse longitude (°) for pulse phases where the linear polarization exceeds the off-pulse *rms*. Three different rotating vector models are shown, corresponding to $\alpha = 30, 60, 90°$. The legend below the figure identifies each curve with the parameters of the associated model. The phase offset ϕ_0, magnetic inclination α, impact parameter β, and maximum slope $d\psi/d\phi$ are quoted in degrees, or °/deg. The data do not significantly constrain the geometry of the system. The smoothed polarization profile is displayed at the top of the figure for reference purposes (I, P, V=solid, dotted, and dashed lines, respectively).

The fits to the polarization position angle data do not significantly constrain the geometry, due to the very narrow range of longitudes exhibiting significant linear polarization. Figure 4.2 displays the PPA data at 575 MHz, in conjunction with a variety of rotating vector model fits. The inclination α is not significantly constrained by the data, although formal χ^2 considerations favour an aligned geometry. In the fits presented in Figure 4.2, the center of symmetry of the PPA curve is located near the center of the available PPA data (at the leading edge of the sharp trailing component). This provides a lower limit on the absolute value of the maximum slope $(d\psi/d\phi)_{max} \sim -2.4 \pm 0.2$. If the symmetry center of the PPA data is not at the

center of the data, then the data do not lie along the portion of the curve with maximum slope. The relativistic correction to the rotating vector model (Blaskiewicz *et al.* 1991) predicts that the symmetry center of the PPA curve will be delayed relative to the symmetry center of the pulse intensity profile, while for emission near the light cylinder, the magnetic field configuration predicts that it will precede the center of the total intensity (Barnard 1986). The narrow range in longitude of the PPA data, combined with the unusual pulse profile, makes confirmation or exclusion of either effect impossible. The 820-MHz and 1410-MHz PPA data provide no further useful information.

For slow pulsars, the width of core components is proportional to $P^{-1/2}/\sin\alpha$ (Rankin 1990). The width of the broad central component in this pulsar is more or less consistent with the expected value at this spin period, for $\alpha \sim 90°$. The other components are all narrower than the predicted core width. A similar relationship is true for the separations of conal components in slow pulsars. Extrapolation to 3 milliseconds yields the expectation that the inner and outer cones should have diameters of $\sim 160°/\sin\alpha$ and $\sim 210°/\sin\alpha$, respectively. If the outer components in this profile are a conal pair, then the observed separation requires (to be consistent with this relationship), $\alpha \sim 35°$ for the inner cone, or $25°$ for the outer cone. These values are consistent with the aligned geometry which is slightly preferred in the fits to the PPA data. Caution should, however, be exercised when extending the relationship for conal separations to periods where the conal diameter is $> 180°$

4.2.2   PSR J1012+5309

This millisecond pulsar has a binary companion with an orbital period of 14.5 hours. The mass function gives an estimate of $M_c = 0.11 M_\odot/\sin i$ for a neutron star mass of $1.4 M_\odot$ (Nicastro *et al.* 1995). Based on optical observations, the white dwarf mass is $0.16 \pm 0.02 M_\odot$ (van Kerkwijk *et al.* 1996), which gives an inclination of $i = \alpha \sim 45°$. The ratio of masses M_{NS}/M_c is also constrained by these observations, however, and this provides a somewhat different estimate of $\alpha \sim 65°$, since the resulting formal value for the neutron star mass is above $2 M_\odot$. The uncertainties in M_c and the mass ratio are such that at the 95% confidence limit the inclination is $50 \lesssim \alpha \lesssim 90°$. This is consistent with the suggestion of Backer (1998) that objects in this class are orthogonal rotators. The white dwarf mass-orbital period relationship of Rappaport *et al.* (1995) is invalid for orbital periods less than a day, such as this one.

Few clues to the geometry are available based on the frequency evolution of the pulse profile. Figure 4.3 highlights the relevant features. The MP and IPb are separated by close to 180°, indicating a possible pulse-interpulse morphology, but the
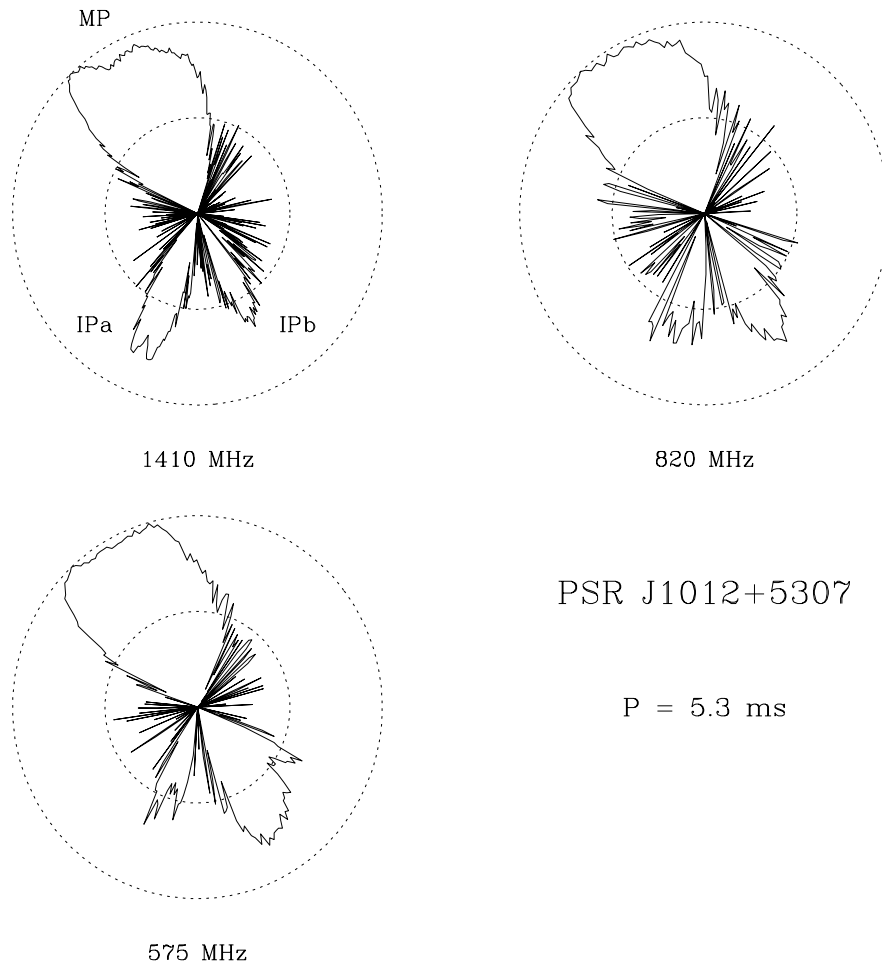
1410 MHz

820 MHz

PSR J1012+5307

P = 5.3 ms

575 MHz

Fig. 4.3.— The relative intensity of PSR J1012+5307 is presented at each radio frequency in a log-polar plot. The main pulse (MP) and IPb are separated by nearly 180°. Emission is present throughout a significant fraction of the pulse period. See the caption of Figure 4.1 for details.

large number of components indicates a possible aligned geometry. Sense-reversing circular is to some degree present under all three structures and cannot therefore be taken as an indication of a central core component. The frequency evolution of the profile does not fall into any standard classification.

Xilouris *et al.* (1998) fit a model of $\alpha \sim 88°$, $\beta \sim 5°$ to this pulsar at 1410 MHz, with the center of symmetry located between the main pulse and IPa. One of the fits displayed in Figure 4.4 (dotted line) represents a similar model. The 1410-MHz data provides the most severe constraints on the model, due to the low linear polarization of IPa at lower frequencies. A significantly better model can be obtained at all radio frequencies by rotating the PPA data for the interpulse structures by 90°, under the assumption that an unseen orthogonal mode transition is present. These data are represented by the open squares in Figure 4.4. A fit for $\alpha = 40°$, $\beta \sim 11°$ provides

PSR J1012+5307 — 1410 MHz

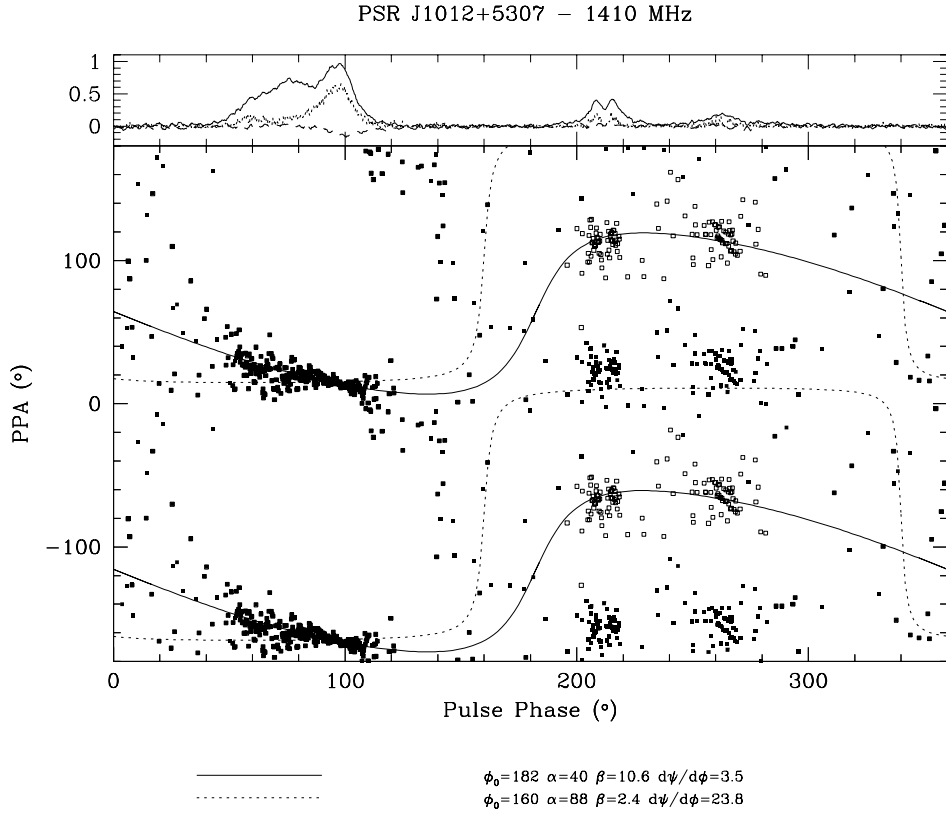φ₀=182 α=40 β=10.6 dψ/dφ=3.5
φ₀=160 α=88 β=2.4 dψ/dφ=23.8

Fig. 4.4.— Rotating vector models are fit to the PPA data of PSR J1012+5307 at 1410 MHz. The data (filled squares) are plotted against pulse longitude (°) for pulse phases where the linear polarization exceeds the off-pulse *rms*. Two different models are shown. One model (dotted line) corresponds to an orthogonal rotator. For the second model (solid line), the data for the interpulse structures have1 been offset by 90° (open squares), under the assumption that an unidentified orthogonal mode is present. This model has $\alpha = 40°$, $\beta \sim 11°$. The smoothed polarization profile is displayed at the top of the figure for reference purposes (I, P, V=solid, dotted, and dashed lines, respectively).

a good fit to the data. The center of symmetry of the PPA curve lies approximately midway between the main pulse and IPb, indicating that this is perhaps a hollow cone system. The slope of the PPA curve at this point is $\sim 3.4°/\mathrm{deg}$.

In either of these models, the maximum slope of the PPA curve $(d\psi/d\phi)_{max}$ occurs between the main pulse and IPa, and is significantly greater than the slope of the observed PPA data ($\sim -0.5°/\mathrm{deg}$ under the MP). The PPA data are difficult to explain using a model with the symmetry center under one of the components.

Based on Rankin's (1993) relation for slow pulsars, the inner and outer conal diameters are expected to be $W_i \sim 8.6°P^{-1/2}/\sin\alpha \sim 120°/\sin\alpha$ and $W_o \sim$

$11.5° P^{-1/2} / \sin \alpha \sim 160° / \sin \alpha$, if the emission occurs at a similar altitude. If both magnetic poles produce radio emission, then the large angular extent of the open-field line region in millisecond pulsars makes it difficult to determine which components originate at a given pole. This complicates the analysis of component separations in complex pulse profiles. Nonetheless, for $\alpha = 90°$, the MP-IPa separation (components 1 to 5/6 in Figure 3.4) of $\sim 120°$ is comparable to the full size of the inner cone. Similarly, the $\sim 165°$ MP-IPb (components 1-4) separation is comparable to the full extent of the outer cone for an orthogonal rotator. The component separations are therefore consistent in the case of an orthogonal rotator. For $\alpha \sim 40°$, as is true for the fit represented by a solid line in Figure 4.4, the IPa-MP separation of $\sim 360 - 120 = 240°$ corresponds to a beam width of $\sim 160°$, comparable to the full size of the outer cone, where we now consider that the components are actually coming from the pole $180°$ away. The IPb-MP separation is in this case $\sim 195°$, corresponding to a beam size of $\sim 125°$, comparable to the size of the inner cone. The IPb-component 2 separation is $\sim 175°$, corresponding to a beam size of $\sim 110°$, again consistent with the size of the inner cone. The conal beam size and rotating vector model geometry are therefore also consistent for $\alpha \sim 40°$. Apart from the broad component 2, all components in this profile are narrower than the core-width relation for slow pulsars would predict.

A magnetic inclination $\alpha = 40°$ lies outside the 95% confidence limits placed on the orbital inclination i by observations of the masses in the system. This discrepancy can be resolved if the orbital and angular momentum axes are not completely aligned. A fit for $\alpha = 50°$ is somewhat compatible with our data, although the PPA offset between the MP and IPa cannot be matched perfectly. This could be explained if the presumed orthogonal mode change were not exactly $90°$, as is seen in some slow pulsars.
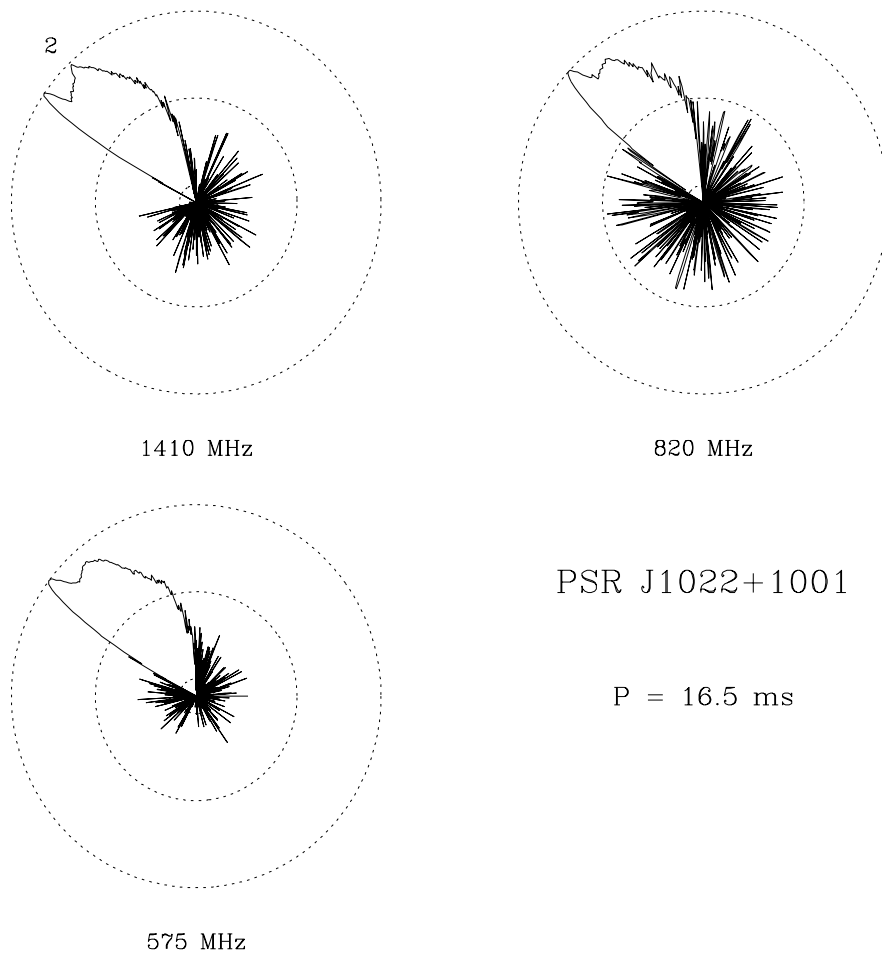
Fig. 4.5.— The relative intensity of PSR J1022+1001 is presented at each radio frequency in a log-polar plot. The intensity, on a logarithmic scale, is presented (solid lines) in polar coordinates, using pulse phase as the angle. Component 2 in the fits of Chapter 3 is identified in the 1410-MHz data. The dotted circles represent the levels of maximum emission, 10%, and 1% of this value.

4.2.3   PSR J1022+1001

This 16 millisecond pulsar has a companion with $M_c \sim 0.73 M_\odot / \sin i$ in a 7.8 day orbit (Camilo *et al.* 1996). This object was not included in the analysis of Backer (1998), due to the large companion mass. If the orthogonal rotator hypothesis applies to some millisecond pulsars, however, it may very well apply to all. The profile evolves very little with frequency (Figure 4.5), so few clues to the geometry are provided. Fortuitously, the PPA data for this pulsar are perhaps the most unambiguous in our data set. A clear sweep in polarization position angle is present across the pulse, although it is disturbed at all frequencies by an orthogonal mode change which occurs over a very narrow range in longitude.

Xilouris *et al.* (1998) found $\alpha \sim 53.2°$, $\beta \sim 7.3°$ at 1410 MHz. In the fits presented

PSR J1022+1001 − 575 MHz

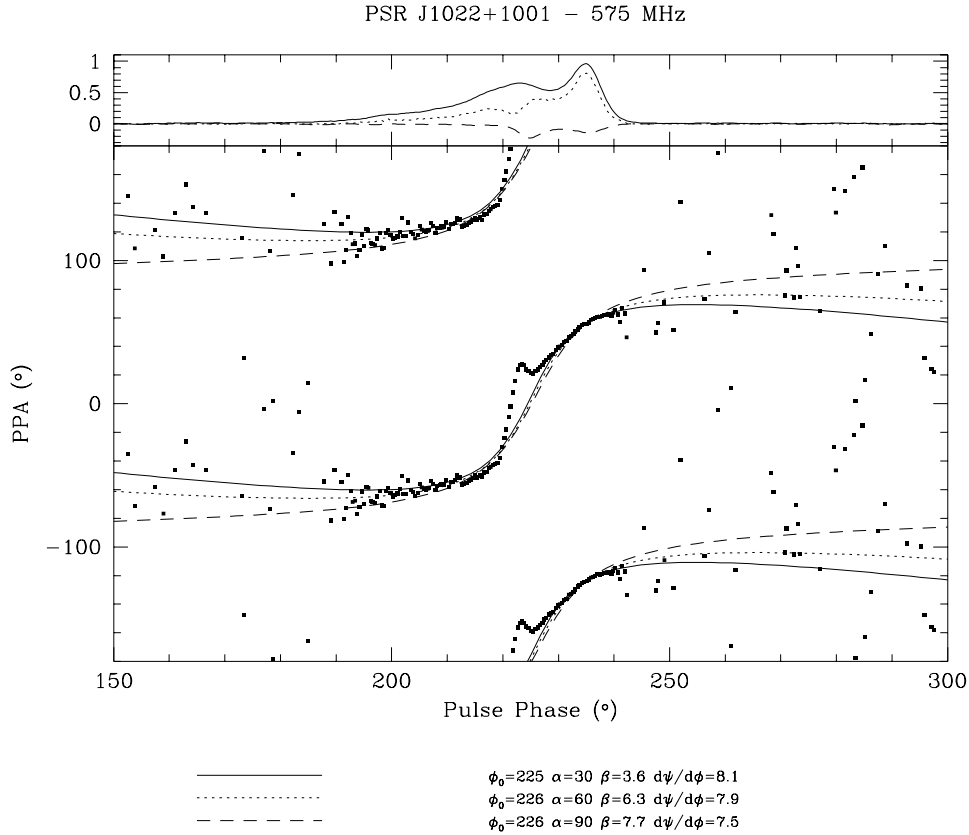|	$\phi_0=225$ $\alpha=30$ $\beta=3.6$ $d\psi/d\phi=8.1$
	$\phi_0=226$ $\alpha=60$ $\beta=6.3$ $d\psi/d\phi=7.9$
	$\phi_0=226$ $\alpha=90$ $\beta=7.7$ $d\psi/d\phi=7.5$

Fig. 4.6.— Rotating vector models are fit to the PPA data of PSR J1022+1001 at 575 MHz. The data (filled squares) are plotted against pulse longitude (°) for pulse phases where the linear polarization exceeds the off-pulse *rms*. A rapid orthogonal mode transition disturbs the data near the center. Models for three values of α are shown. Among those shown, the model with $\alpha = 60°$, $\beta \sim 6.3°$ is preferred. The smoothed polarization profile is displayed at the top of the figure for reference purposes (I, P, V=solid, dotted, and dashed lines, respectively).

here, no correction has been made for the presence of the orthogonal mode in the PPA data, under the assumption that the accompanying depolarization will sufficiently suppress the weight of these data. At 575 MHz, the depolarization accompanying the mode transition was not sufficient to suppress these PPA data relative to that in the leading portion of the profile, so more parameters were held fixed in the fit than was usual. The results of the 575-MHz fits are shown in Figure 4.6, for $\alpha = 30°, 60°$,and 90°. In all cases, the maximum slope is $(d\psi/d\phi)_{max} \sim 8°/\text{deg}$, and the center of symmetry lies below component 2, which is near the symmetry center of the profile (cf. Figures 3.7 and 4.5). The model with $\alpha = 60°$, $\beta \sim 6°$ is preferred on the basis of the PPA data at the edges of the profile. At 1410 MHz, the leading edge of the profile suggests that larger α may be preferable (cf. Figure 4.7), while $\alpha = 60°$ is
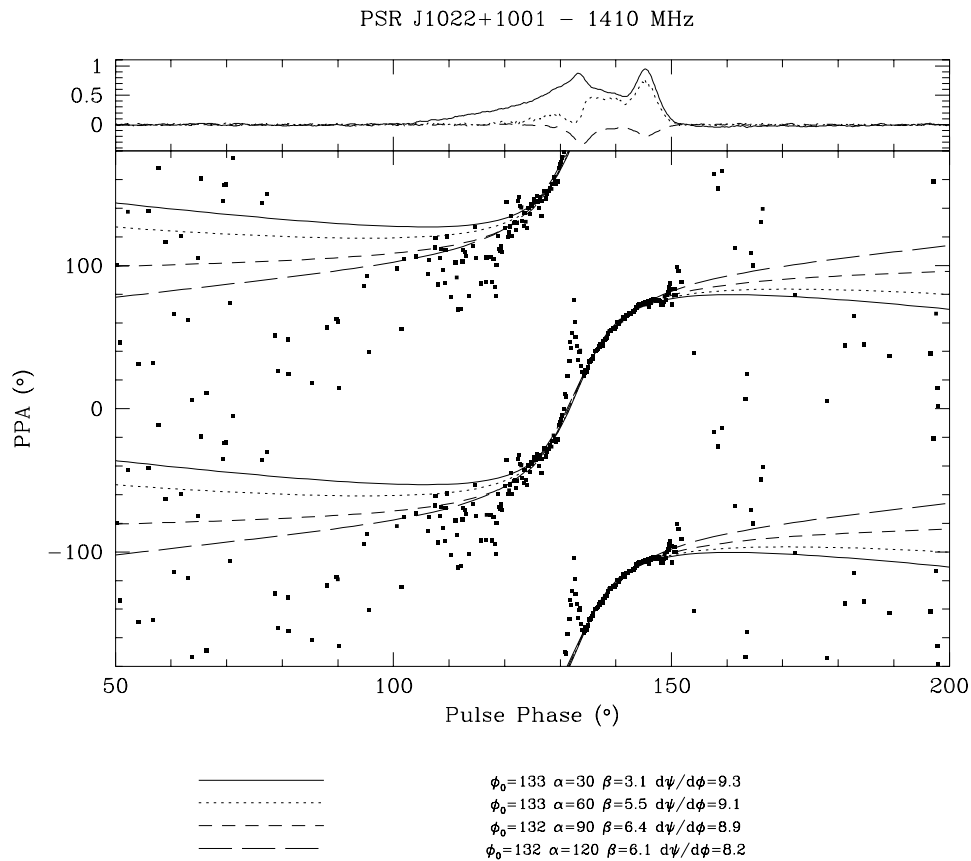
PSR J1022+1001 − 1410 MHz

Fig. 4.7.— Rotating vector models are fit to the PPA data of PSR J1022+1001 at 1410 MHz. The data (filled squares) are plotted against pulse longitude (°) for pulse phases where the linear polarization exceeds the off-pulse rms. The orthogonal mode is once again clearly visible in the data. Models for four values of α are shown. The smoothed polarization profile is displayed at the top of the figure for reference purposes (I, P, V=solid, dotted, and dashed lines, respectively).

satisfactory on the trailing edge. However, this is less true for the PPA data if no correction for instrumental cross-coupling ($\sigma \neq 0$) has been done. The contradictory result is likely due to the non-linear effects of an error in our correction for σ, as the linear polarization is extremely small in this section of the pulse profile (cf. Section 2.5). The maximum slope in this case is $\sim 9°$. The 820-MHz data do not significantly constrain our results.
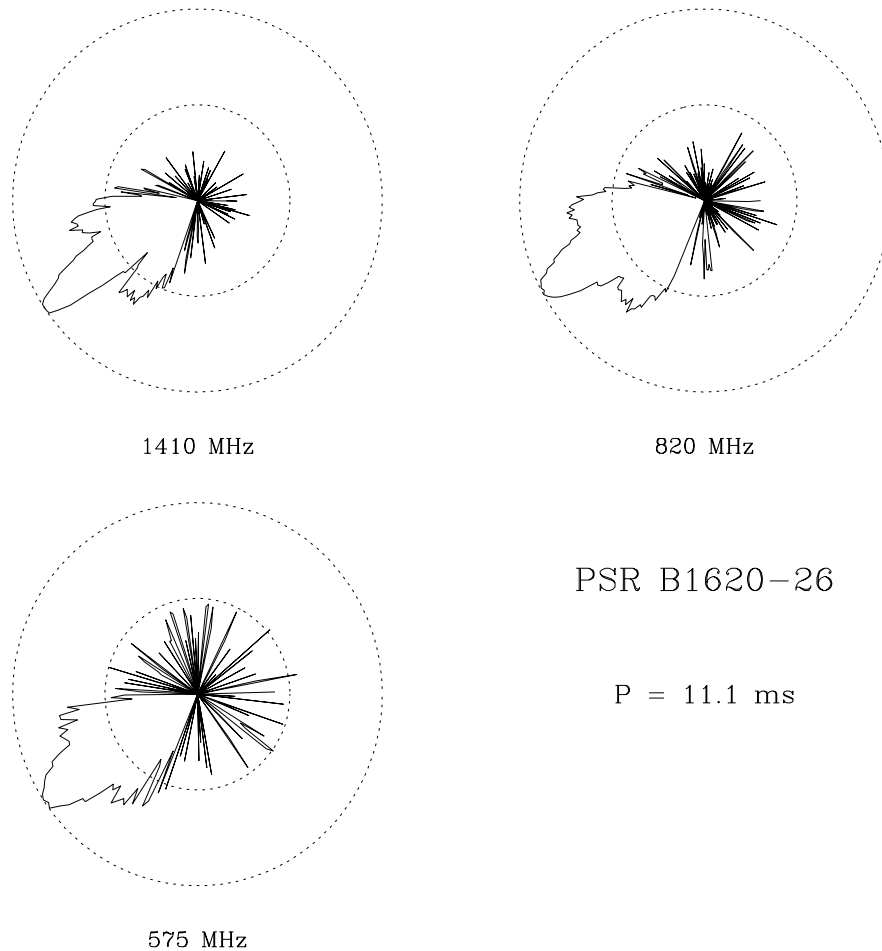
1410 MHz

820 MHz

PSR B1620−26

P = 11.1 ms

575 MHz

Fig. 4.8.— The relative intensity of PSR B1620−26 is presented at each radio frequency in a log-polar plot. See caption of Figure 4.1 for details.

4.2.4   PSR B1620−26

This pulsar, located in the globular cluster M4 (Lyne *et al.* 1988) has a 0.3 $M_\odot / \sin i$ companion in a 191 day orbit, plus a second companion in a wide outer orbit (Backer, Foster & Sallmen 1993). The orbital period-companion mass relation predicts an inclination $i = \alpha \sim 45°$ for alignment of the orbital and spin angular momentum axes. This relation may not apply in this case, however, since the history of the binary system may be significantly influenced by encounters with other stars in the globular cluster.

The profile resembles a triple profile consisting of a core component with conal outriders, but the core component is stronger at higher frequencies, contrary to expectations (see Figure 4.8). This component is also somewhat narrower than that expected on the basis of the width-period relationship from slow pulsars. On the
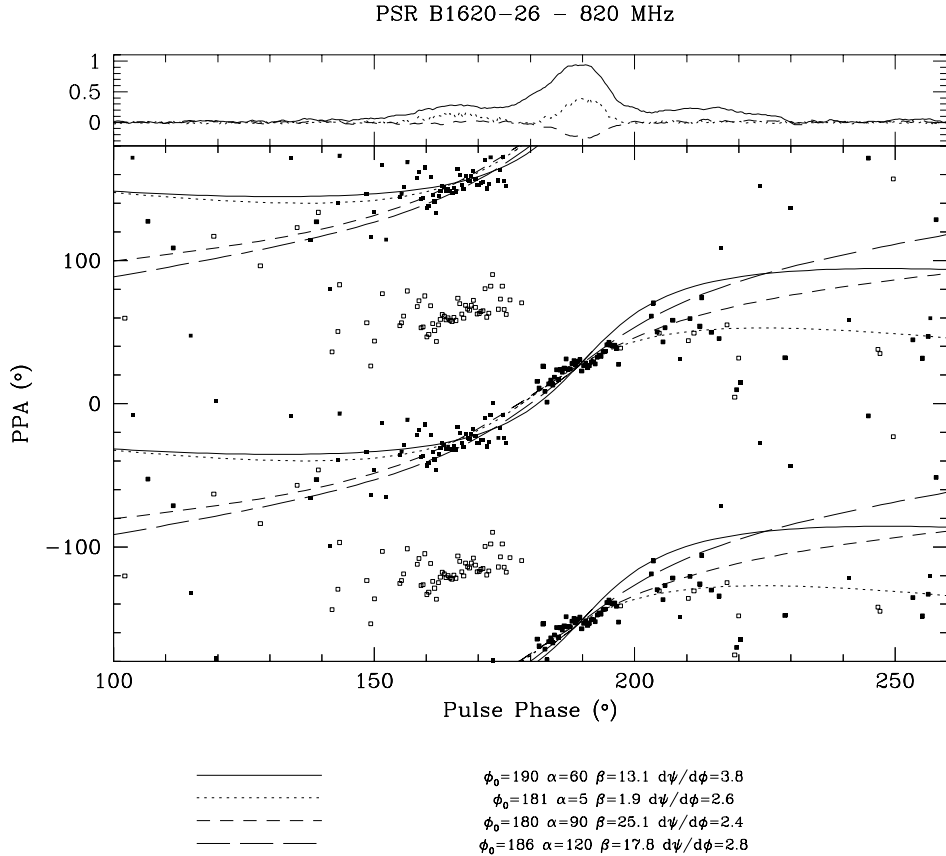
PSR B1620−26 − 820 MHz

————————	$\phi_0=190\ \alpha=60\ \beta=13.1\ d\psi/d\phi=3.8$
····················	$\phi_0=181\ \alpha=5\ \beta=1.9\ d\psi/d\phi=2.6$
– – – – –	$\phi_0=180\ \alpha=90\ \beta=25.1\ d\psi/d\phi=2.4$
— — —	$\phi_0=186\ \alpha=120\ \beta=17.8\ d\psi/d\phi=2.8$

Fig. 4.9.— Rotating vector models are fit to the PPA data of PSR B1620−26 at 820 MHz. The data (filled squares) are plotted against pulse longitude (°) for pulse phases where the linear polarization exceeds the off-pulse *rms*. An orthogonal mode transition has been removed. The original data are shown by open squares. Four different models are shown. The solid line represents a model in which the symmetry center was forced to lie under the (presumed) central core component. In the remaining three models, the symmetry center lies near the center of the available PPA data. The smoothed polarization profile is displayed at the top of the figure for reference purposes (I, P, V=solid, dotted, and dashed lines, respectively).

other hand, the predicted diameter of an inner cone, which is 80° at this spin period, is consistent with the observed separations for $\alpha \sim 30°$.

For the fits presented for this object, the PPA data preceding the observed orthogonal mode transition were shifted by 90°. The 820-MHz data provides the best constraint on the pulsar geometry. Figure 4.9 shows the results of fits for $\alpha = 5°, 90°$, and 120°. Their center of symmetry is located in the middle of the PPA data, near the location of the orthogonal mode transition, and preceding the symmetry center of the intensity profile by $\sim 15°$. Many values of α are acceptable, due to the small range in pulse longitude covered by the PPA data. In fact, the 1410-MHz data are

consistent with values for the inclination ranging from 5 to 150°. A χ^2 analysis at 820-MHz indicates that an aligned geometry is somewhat preferred. The maximum slope is 2.5 ± 0.2, based on the 820-MHz and 1410-MHz data. The 575-MHz data is of poorer quality. A fourth fit is presented (solid line), where the symmetry center of the profile lies under the central component, and $\alpha = 60°$. In this case, the maximum slope is $\sim 3.8°/\text{deg}$. This model does not fit the data as well. If the symmetry center of the PPA curve truly precedes that of the intensity profile, it suggests that the emission occurs near the light cylinder, where the azimuthal component of the magnetic field has a significant effect. The values for the maximum slopes may be biased if the mode transition were not truly orthogonal. A slight offset between the two portions of the PPA data suggests that this might be the case. If true, the maximum slopes are smaller than those quoted here. The transition may also be truly orthogonal, with the apparent offset due entirely to the missing data accompanying the mode transition. The depolarization accompanying this "orthogonal" mode makes it difficult to determine the behaviour of the PPA in this region. If this were possible, the ambiguity might be resolved.
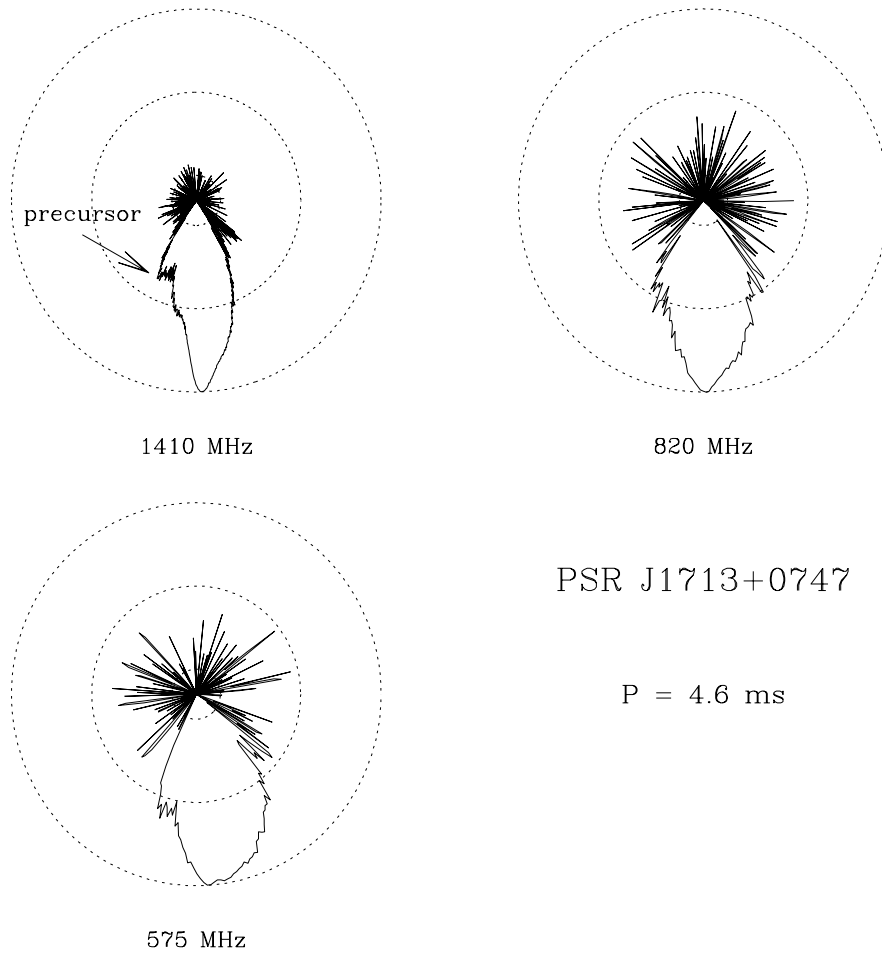
Fig. 4.10.— The relative intensity of PSR J1713+0747 is presented at each radio frequency in a log-polar plot. See caption of Figure 4.5 for details.

4.2.5   PSR J1713+0747

The overall extent of the emission beam in this pulsar appears to decrease significantly with increasing frequency (cf. Figure 4.10), although the results of component fitting in Chapter 3 suggest that this is probably due to the increased dominance of the central component relative to the others, rather than a change in the size of the emission region. The many components of the profile are difficult to classify, although sense-reversing circular polarization under the main pulse indicates that this is a core component. The components of this profile are, however, all narrower than the predicted core component width at this spin period. The separation of the main pulse and the trailing component (components 1-4 in Figure 3.13) is $\sim 45°$, which is narrower than the predicted radius of the inner hollow cone. The classification of components within this profile is uncertain.
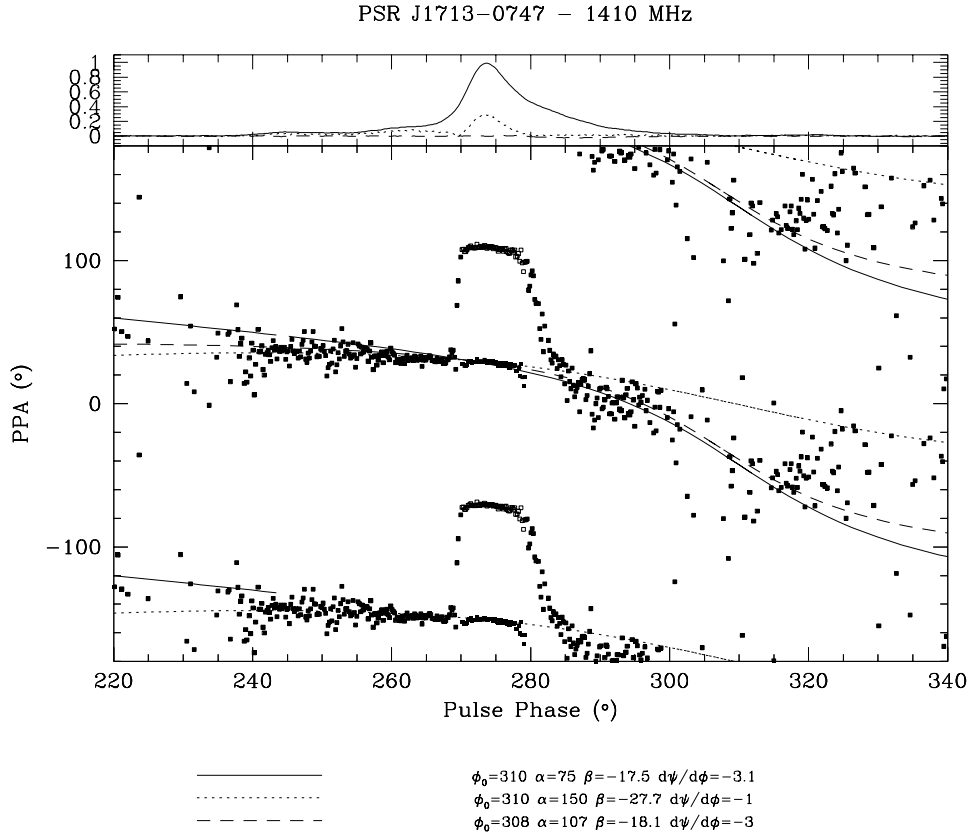
PSR J1713-0747 - 1410 MHz

Fig. 4.11.— Rotating vector models are fit to the PPA data of PSR J1713+0747 at 1410 MHz. The data (filled squares) are plotted against pulse longitude (°) for pulse phases where the linear polarization exceeds the off-pulse *rms*. An orthogonal mode transition has been removed. The original data are represented by open squares. Three different rotating vector models are shown. The smoothed polarization profile is displayed at the top of the figure for reference purposes (I, P, V=solid, dotted, and dashed lines, respectively).

This 4.5-millisecond pulsar has a companion in a wide, circular, 67.8-day orbit (Foster *et al.* 1993). The pulses are delayed by the effects of general relativity as they pass the companion, and measurement of this Shapiro delay allows an estimate of the orbital inclination. These measurements suggest a companion mass of $0.33 M_\odot$, and the inclination angle is restricted to the range 57° to 81° by requiring that the neutron star mass be $\lesssim 3 M_\odot$ (Camilo *et al.* 1994). Non-aligned geometries are preferred. The relation of Rappaport *et al.* suggests $i = 56.5°$, which is just barely consistent with this measurement.

An orthogonal mode transition has been removed from the data presented in Figure 4.11. The apparent sharp sweep which remains is an artifact due to the low linear polarization accompanying the mode transition, and the non-linear effects of

the instrumental parameter σ for $P/I << 1$ (cf. Section 2.5). The remaining PPA data are relatively flat under the main portion of the pulse, with a slope that increases on the trailing edge of the pulse. Data which have had no correction for $\sigma \neq 0$ also show this trend on the trailing edge of the pulse. The 1410-MHz data provides the strongest constraints on the PPA curve, although all frequencies are consistent with the results presented here. Figure 4.11 displays the results of three fits, for $\alpha = 75°$, 105°, and 150°. The best results are obtained for α near 105°, or 75° measured relative to the other rotation axis. This is consistent with the Shapiro delay measurement. The center of symmetry of the PPA model trails the main pulse by $\sim 30°$, which would indicate an emission radius of $R_e = c\Delta t/4 = 0.13 r_{LC} = 28$ km if it is due to relativistic effects. The maximum slope is $\sim -3°/\text{deg}$.

1410 MHz

820 MHz

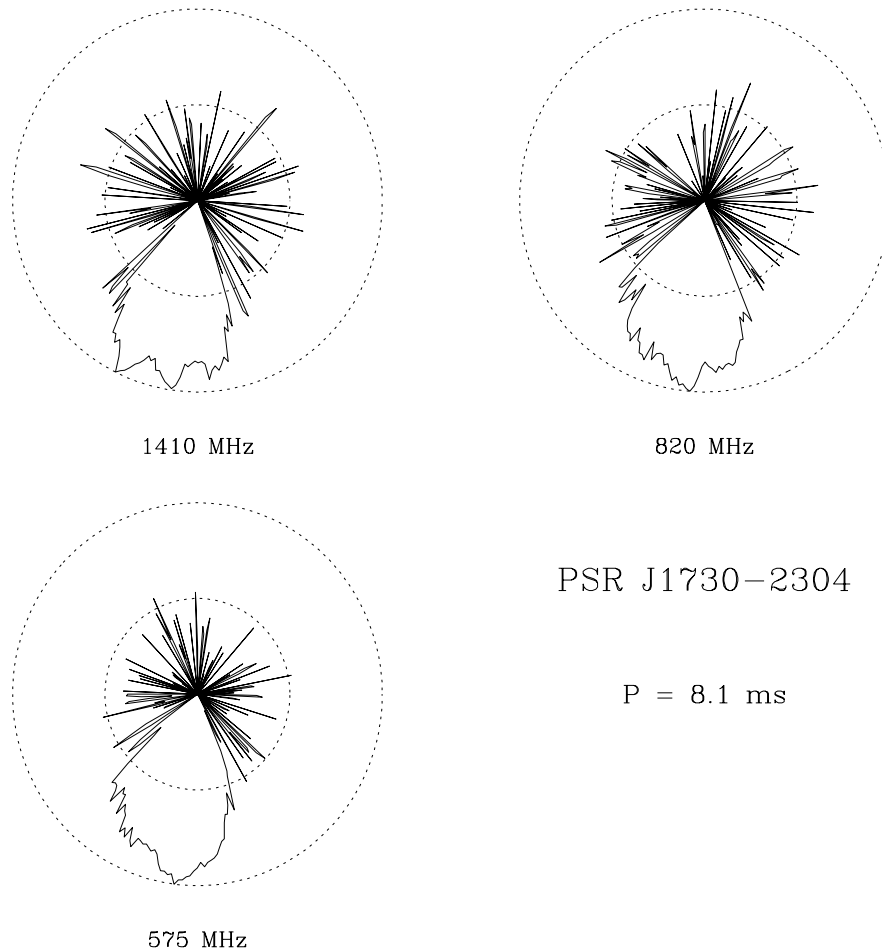PSR J1730−2304

P = 8.1 ms

575 MHz

Fig. 4.12.— The relative intensity of PSR J1730−2304 is presented at each radio frequency in a log-polar plot. See caption of Figure 4.1 for details.

4.2.6   PSR J1730−2304

This 8-millisecond pulsar has no companion. The PPA data are confined to a very narrow range of pulse longitudes. Therefore the geometry cannot be easily determined from a rotating vector model. The frequency evolution of the intensity profile is as expected for a symmetric multiple component profile, indicating that the central component may be identified as a core component (cf. Figure 4.12). However, all components are narrower than is expected on the basis of the core width-period relation. The center of symmetry is expected to lie at the pulse phase of the core component, apart from relativistic effects and magnetic field distortion near the light cylinder. The PPA data, which lie under the trailing component, have a slope of $\sim -1.0°/\mathrm{deg}$ at 820 MHz. Figure 4.13 displays the rotating vector model for a variety of values of α. The fits are poorly constrained by the data.

PSR J1730−2304 − 820 MHz

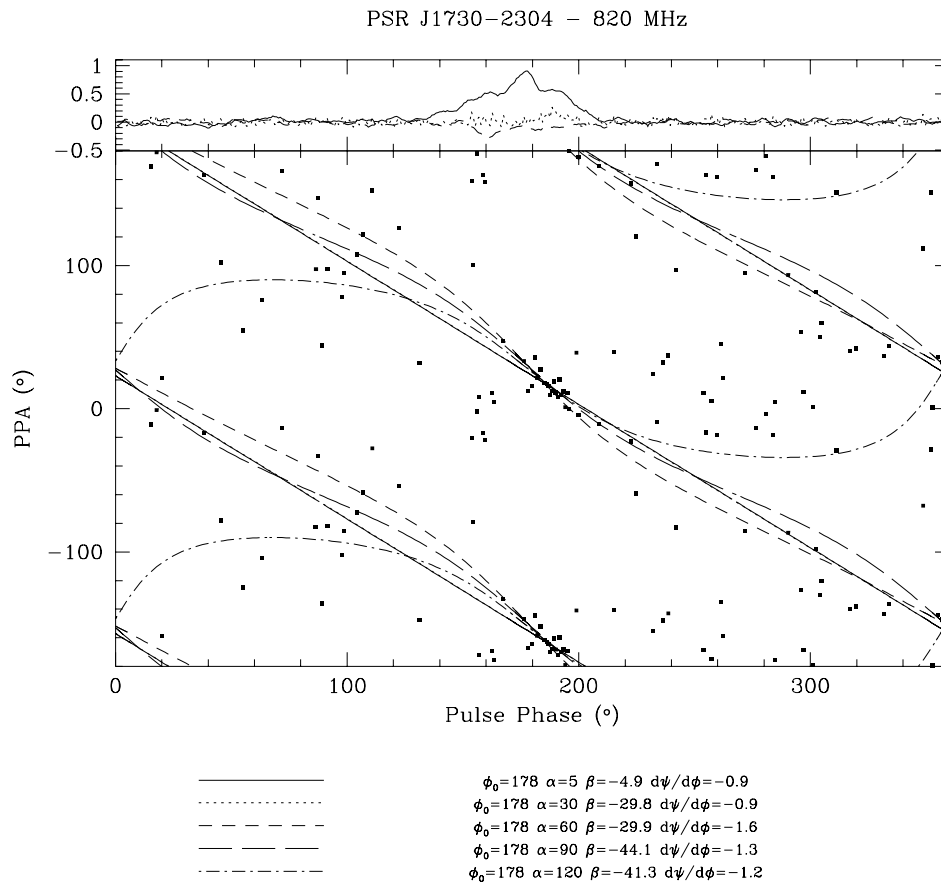|	
———————	ϕ_0=178 α=5 β=−4.9 dψ/dϕ=−0.9
··················	ϕ_0=178 α=30 β=−29.8 dψ/dϕ=−0.9
− − − − −	ϕ_0=178 α=60 β=−29.9 dψ/dϕ=−1.6
— — —	ϕ_0=178 α=90 β=−44.1 dψ/dϕ=−1.3
−·−·−·−	ϕ_0=178 α=120 β=−41.3 dψ/dϕ=−1.2

Fig. 4.13.— Rotating vector models are fit to the PPA data of PSR J1730−2304 at 820 MHz. The data (filled squares) are plotted against pulse longitude (°) for pulse phases where the linear polarization exceeds the off-pulse *rms*. Five different models are shown, indicating that the magnetic inclination α is poorly constrained. The smoothed polarization profile is displayed at the top of the figure for reference purposes (I, P, V=solid, dotted, and dashed lines, respectively).

4.2.7   PSR B1821−24

The profile of this isolated 3-millisecond pulsar does not fall easily into the usual classification schemes. The sharp components are significantly narrower than that expected on the basis of the core-width relation for slow pulsars. The intrinsic width of the trailing broad component is difficult to determine accurately, since the components are broadened by interstellar scattering at the lower radio frequencies, and it has faded significantly at 1410 MHz. With this caveat, the 1410-MHz width determined through component fitting is still narrower than the expected core width at this spin period (cf. Chapter 3).

Due to the approximately 180° separation between components 1 and 3 (cf. Figures 3.20 and 4.14), Backer & Sallmen (1997) suggested a two-pole model for this

1410 MHz

820 MHz

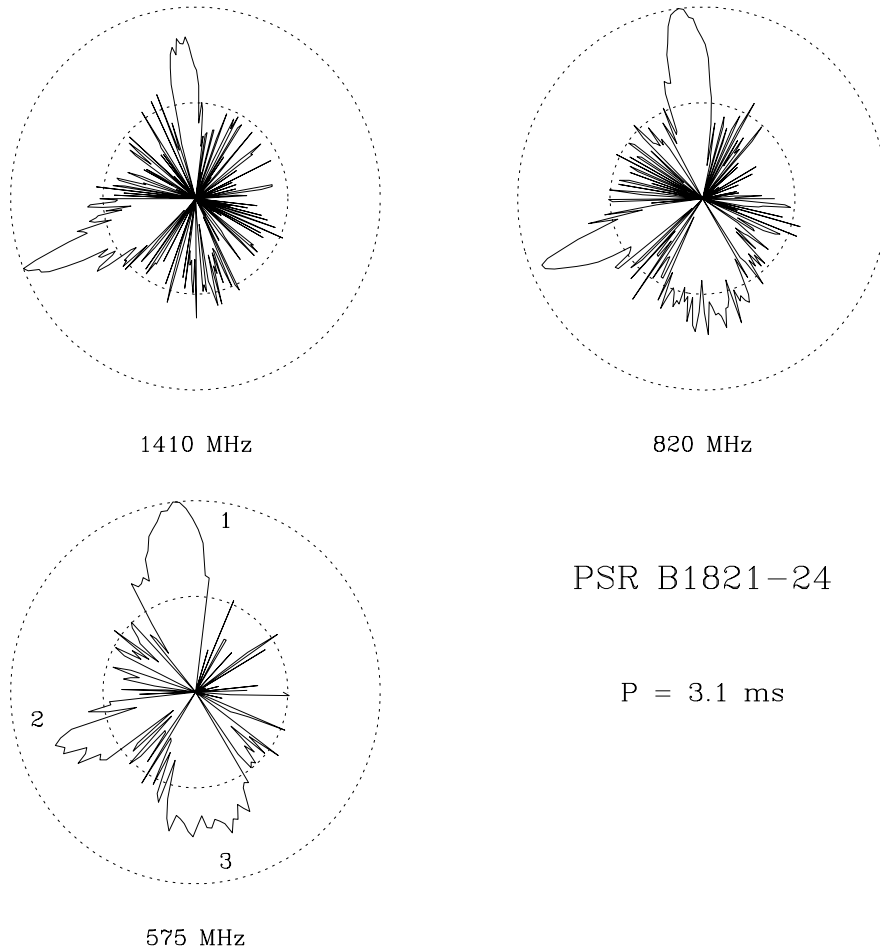PSR B1821−24

P = 3.1 ms

575 MHz

Fig. 4.14.— The relative intensity of PSR B1821−24 is presented at each radio frequency in a log-polar plot. The component numbers from the fits discussed in Chapter **3** are used to identify the components in the 575-MHz plot. See caption of Figure 4.1 for details.

pulsar. Assuming that component 1 is associated with one pole of the pulsar, a rotating vector model with $\alpha = 50°$, $\beta \sim 40°$ was fit to the 820-MHz data to match the slope of the main pulse PPA data ($\sim 1°/\text{deg}$) and the relative offset of the PPA data for component two. A similar model is shown in Figure 4.15 for the 1410-MHz data (solid line). The 820-MHz data presented in their paper were a subset of those presented here, and the results do not differ significantly. At 575-MHz, the slope of the main pulse PPA decreases slightly, probably due to the effects of interstellar scattering. In this model, component 2 is a conal outrider to component 1. The separation between the two is $\sim 108°$. This is consistent with the outer conal half-width separation predicted for this inclination α by extrapolating the slow-pulsar relation to this spin period. In this case, however, the full conal diameter is $> 180°$, and extending the relation to this extreme may be invalid.

PSR B1821+21 — 1410 MHz

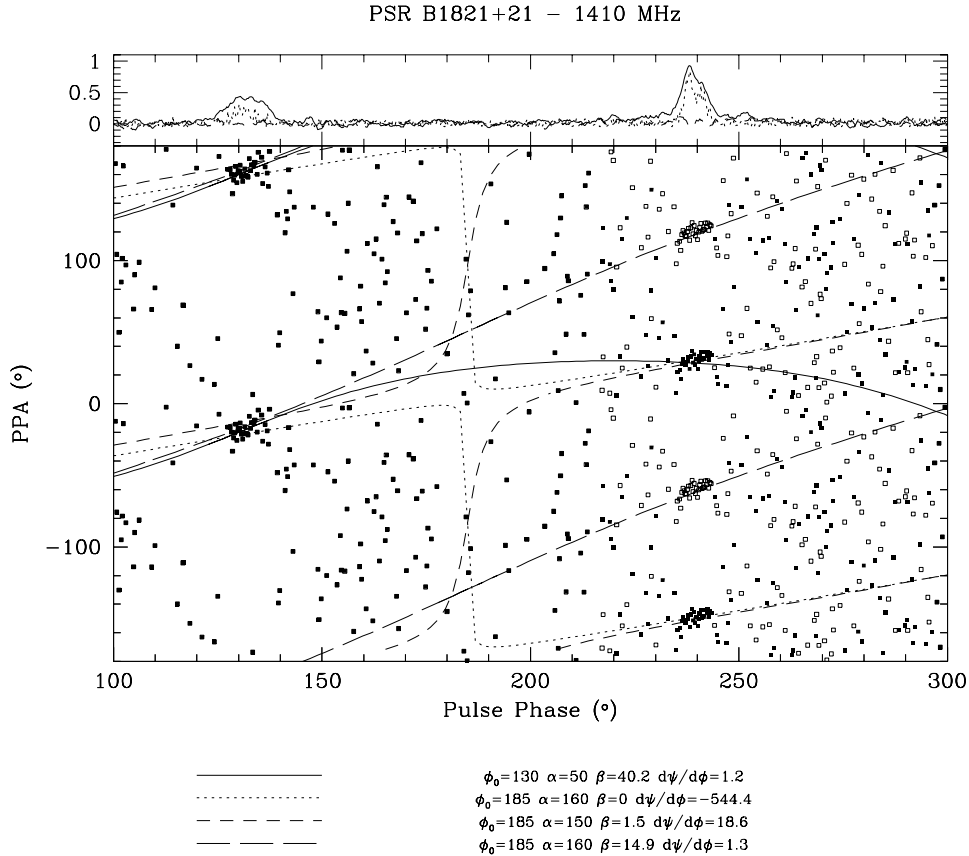|	
————————	ϕ_0=130 α=50 β=40.2 dψ/dϕ=1.2
····················	ϕ_0=185 α=160 β=0 dψ/dϕ=−544.4
— — — — —	ϕ_0=185 α=150 β=1.5 dψ/dϕ=18.6
—— —— ——	ϕ_0=185 α=160 β=14.9 dψ/dϕ=1.3

Fig. 4.15.— Rotating vector models are fit to the PPA data of PSR B1821−24 at 1410 MHz. The PPA data (filled squares) are plotted against pulse longitude (°) for pulse phases where the linear polarization exceeds the off-pulse *rms*. The open squares represent data to which a 90° rotation has been applied. The model associated with the solid line has its symmetry center under the first component, and is relatively well constrained by the PPA slope for this component, and the PPA offset of the other component. The other models have their center of symmetry between the two components, and α is poorly constrained for these cases. The long-dashed line represents a model for the rotated data. The smoothed polarization profile is displayed at the top of the figure for reference purposes (I, P, V=solid, dotted, and dashed lines, respectively).

By placing the center of symmetry between components 1 and 2, it is possible to fit the PPA data for a wide variety of inclinations α. This is also true if the PPA data of component two are shifted by 90° relative to that of component 1, under the assumption that an unobserved orthogonal mode transition occurs. The open squares in Figure 4.15 represent the rotated data. Three models with the symmetry center between components 1 and 2 are shown in Figure 4.15, displaying the insensitivity of the fits to magnetic inclination α. The separation between the two components can be made consistent with the expected inner cone diameter if α is chosen judiciously.

The cusp-like components in this pulsar have led to the suggestion that these are

due to emission in the outer magnetosphere (Chen & Ruderman 1993b, Backer & Sallmen 1997). Chen & Ruderman (1993b) note that the magnitude of the surface magnetic field for this pulsar places it in or near region I in their Figure 2, which is associated with Crab-like outer-magnetospheric emission. Romani & Yadigaroglu (1995) show that widely spaced pairs of components are produced by the outer-gap emission associated with a single pole, and that the "normal" polar cap radio beam (which is from the opposite pole) precedes the outer-gap emission by 0.35-0.50 period. The Crab pulsar has radio emission associated with the high-energy, outer gap radiation, while the Vela pulsar does not. The tentative identification of the observed X-ray components (Saito *et al.* 1997) with components 1 and 3 (Backer & Sallmen 1997) has now been confirmed (Rots *et al.* 1998). The observations would therefore imply that this pulsar also displays outer-magnetospheric emission. Component two is associated with the typical polar cap beam in this model. Intriguingly, the extra broad component required under component 2 in the 1410-MHz fit does have the expected core component width for an inclination of $\alpha \sim 90°$, although the sharp feature superimposed upon it is much narrower. An inconsistency in this picture is that there is non-zero radio emission between components 1 and 3 relative to that between components 3 and 1 (Backer & Sallmen 1997). The reverse is expected to be true in the Romani & Yadigaroglu model. Furthermore, this model predicts cusp-like component profiles for the outer-gap radiation, while we associate the sharp component 2 with the polar cap emission, and the broader component 3 with the outer-gap emission. The PPA data for components 1 and 2 are in many ways similar to that of the MP and IP of the Crab pulsar, exhibiting shallow slopes under two sharp components (cf. Figure 3.33). It is unfortunate that component 3 shows no significant polarization, since PPA data in that longitude region could help to distinguish between various models.

4.2.8   PSR B1937+21

The original millisecond pulsar, PSR B1937+21 is still the most rapidly rotating pulsar known. The MP-IP separation is 173° at all radio frequencies, suggesting a two-pole model for this pulsar (see Figure 4.16). The components are significantly narrower than the predicted core width for an object with this spin period. Once it has been corrected for orthogonal modes, the PPA is very flat, with a slope of $\sim -.5$ to $-1°$/deg under the main pulse. At 1410 MHz, the PPA data for the pulse and interpulse each have a shallow downward trend across the pulse. At 820 MHz and 575 MHz, the IP trend is reduced or even reversed (cf. Figure 4.17). If this effect is real, a single geometric rotating vector model cannot fit the data at all frequencies. The

1410 MHz

820 MHz

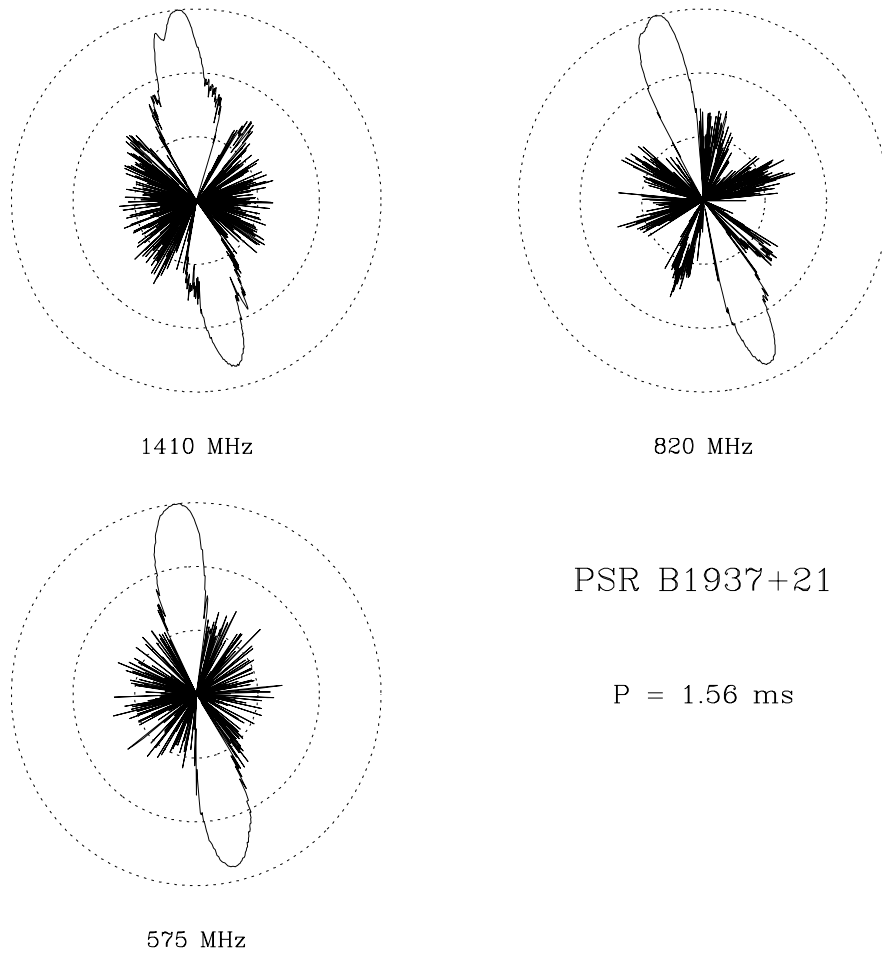PSR B1937+21

P = 1.56 ms

575 MHz

Fig. 4.16.— The relative intensity of PSR B1937+21 is presented at each radio frequency in a log-polar plot. The low-level systematics at 820 MHz and 575 MHz are instrumental effects. See caption of Figure 4.5 for details.

1410-MHz data can be fit by models with a large range in α, centered either under the main pulse, or between the two components. Due to the slope reversal of the IP at lower frequencies, the models required there are significantly different.

In the absence of a rotating vector model, the flat PPAs seen here can be explained in the model of Barnard (1986) by the presence of an azimuthal B field outside the light cylinder. Alternatively, Rankin (1990) suggests that the PPA behaviour of core components is disorderly, and should not be used as an indicator of pulsar geometry.

The MP-IP morphology of this pulsar is similar to that of the Crab pulsar (cf. Figure 3.33). In addition, the PPA data at 1410 MHz strongly resemble that for the MP and IP of the Crab pulsar, which also exhibit a shallow downward trend under each component. This, combined with the fact that these are the only two pulsars known to exhibit giant pulses (cf. Chapter 6), suggests a common source for their
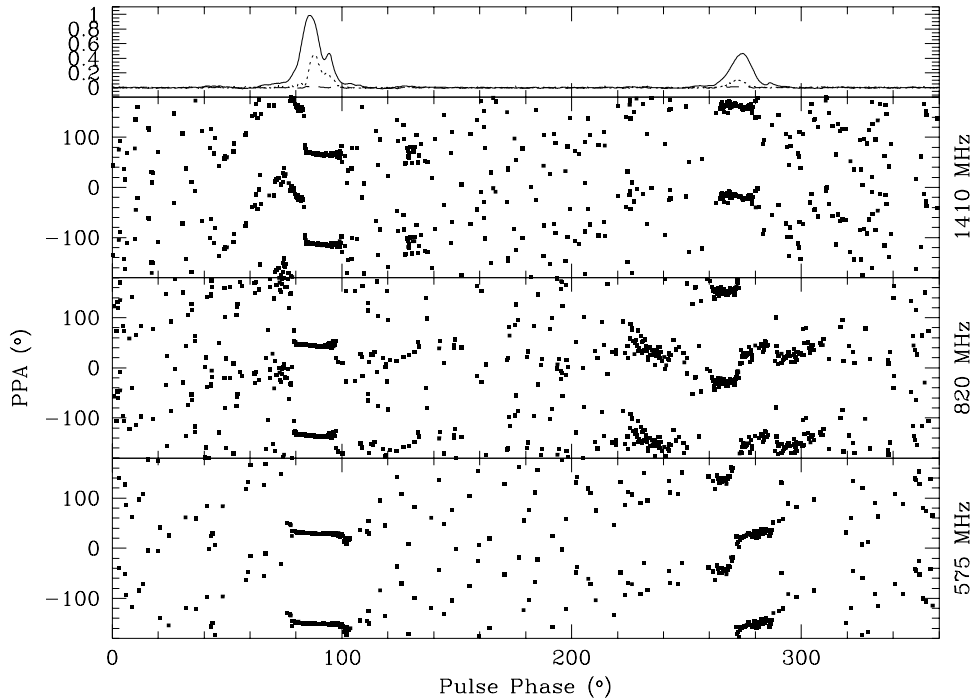
Fig. 4.17.— The PPA data are displayed for PSR B1937+21 at three radio frequencies. The PPA data (filled squares) are plotted against pulse longitude (°) for pulse phases where the linear polarization exceeds the off-pulse *rms*. The data are disturbed by orthogonal mode transitions. Once these have been taken into account, the PPA slope under the main pulse is roughly consistent at all frequencies, but the slope of the IP data changes sign. If this is real, and not due to imperfect calibration, no single simple geometric model can fit all of the data. The off-pulse systematics in the 820-MHz PPA curve are instrumental in origin. The smoothed 1410-MHz polarization profile is displayed at the top of the figure for reference purposes (I, P, V=solid, dotted, and dashed lines, respectively).

emission. The MP and IP in the Crab pulsar are widely believed to originate in an emission region in the outer magnetosphere (*e.g.*, Romani & Yadigaroglu 1995). In the model of Chen & Ruderman (1993b), pulsars which lie in region I of their Figure 2 are expected to produce outer magnetospheric emission. PSR B1937+21 falls in this "Crab-like" region of that figure, indicating outer magnetospheric emission is expected. On the other hand, they note that the component separation is extremely close to 180°, which is not expected for outer magnetospheric emission in their model. They attribute the profile morphology to an unusual magnetic field configuration (Chen & Ruderman 1993a). During prolonged spin-up, the moving crust compresses the surface magnetic field, resulting in a magnetic field centered on the rotation axis
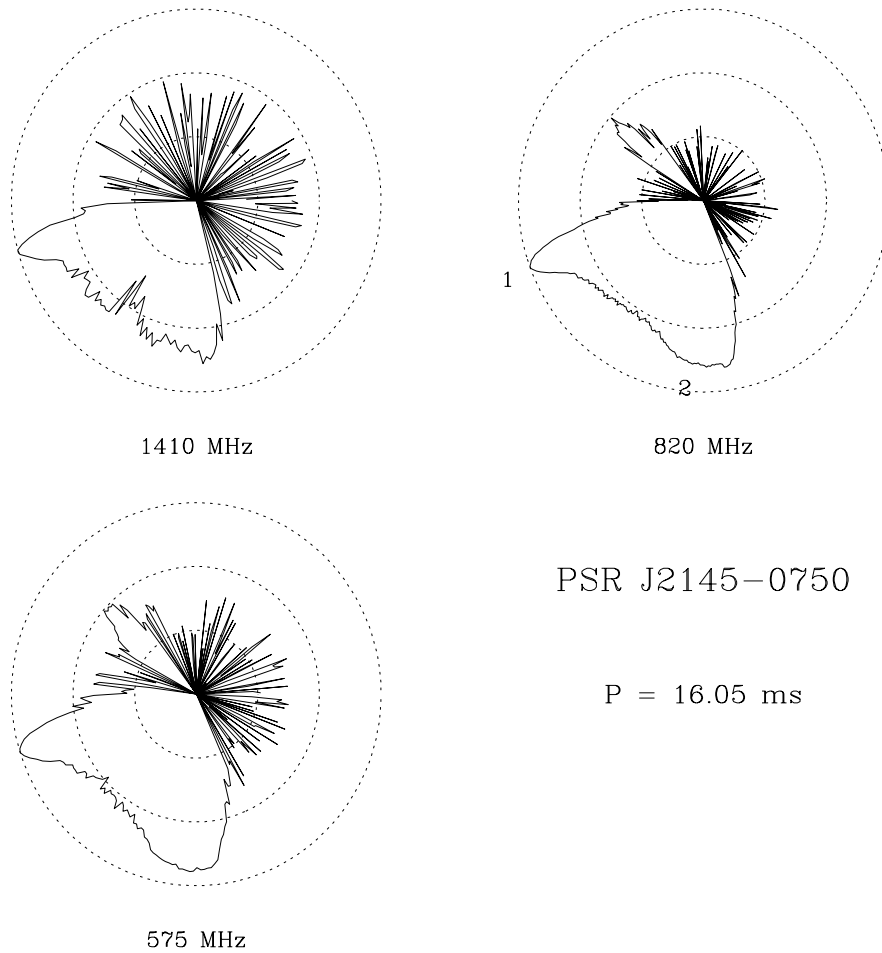
1410 MHz

820 MHz

PSR J2145−0750

P = 16.05 ms

575 MHz

Fig. 4.18.— The relative intensity of PSR J2145−0747 is presented at each radio frequency in a log-polar plot. Components 1 and 2 in the fits described in Chapter 3 are identified in the 820-MHz data. See caption of Figure 4.1 for details.

at the surface, and orthogonal to the rotation axis.

4.2.9 PSR J2145−0750

This 16-millisecond pulsar is in a 6.8-day binary orbit with a $0.51 M_\odot$ white dwarf (optically identified by Bell *et al.* 1995). The mass function for this particular system indicates that the white dwarf has a minimum companion mass incompatible with the theoretical mass-orbital period relation.

The profile here is complex, with many components, and pulsed-emission over a wide fraction of a pulse period (see Figure 4.18). The separation of the two main components is consistent with the extrapolation of the expected inner-cone diameter to this spin period, for $\alpha = 90°$. The precursor and component 2 each exhibit sense-

PSR J2145−0750 − 820 MHz

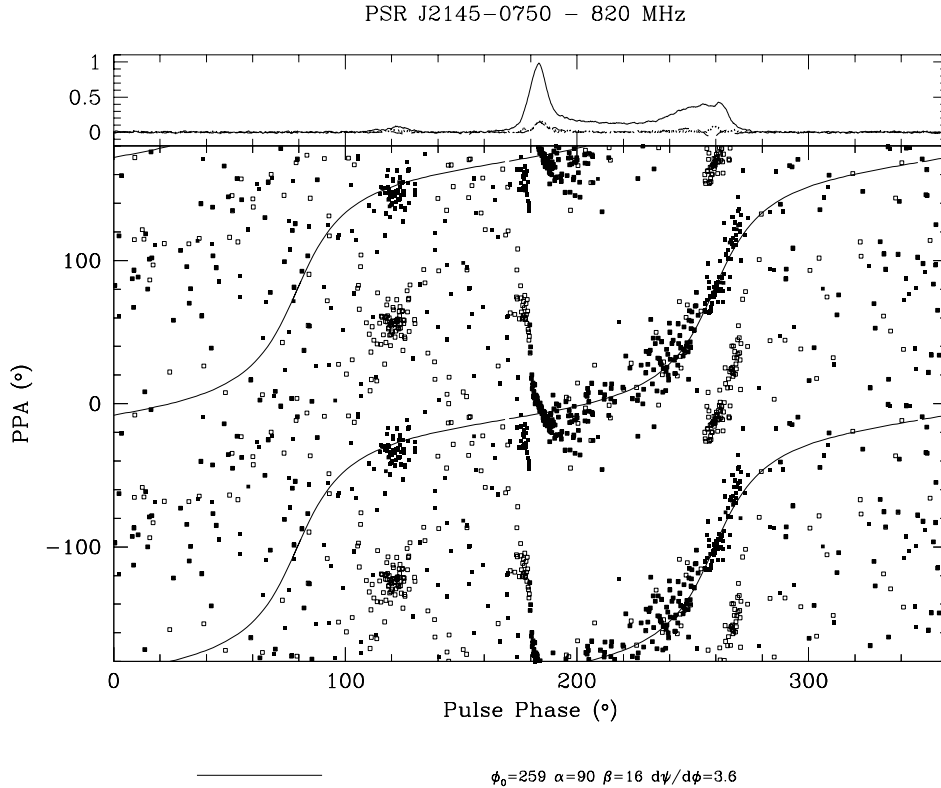ϕ_0=259 α=90 β=16 dψ/dϕ=3.6

Fig. 4.19.— Rotating vector models are fit to the PPA data of PSR J2145−0750 at 1410 MHz. The data (filled squares) are plotted against pulse longitude (°) for pulse phases where the linear polarization exceeds the off-pulse *rms*. Two orthogonal mode changes have been removed from the data. The original data are represented by open squares. The solid line represents a particular rotating vector model. The smoothed polarization profile is displayed at the top of the figure for reference purposes (I, P, V=solid, dotted, and dashed lines, respectively).

reversing circular polarization, which is often a sign of core component emission. Their separation is only ∼ 130°, making it difficult to associate these with opposite magnetic poles in a dipolar field geometry. The FWHM of component 2 is, however, similar to the expected width of a core component for $\alpha = 90°$. Kuzmin & Losovsky (1994) note that the separation of the pulse components *increases* at higher radio frequencies, contrary to expectations. They propose a significant quadrupolar component to the magnetic field, which would be somewhat surprising in light of the results of Arons (1993), which limit the non-dipolar nature of the magnetic field in millisecond pulsars.

The polarization position angle data presented here, although consistent across all frequencies, are complicated. The 820-MHz data were used for the fitting process,

although the 575-MHz PPA data are consistent with the results. The 1410-MHz data were too weakly polarized to be of assistance. For the fit presented in Figure 4.19, correction has been made for two orthogonal mode transitions. The original data are shown by the open squares. The apparent sweep in PPA accompanying the linear depolarization preceding component 1 has been assumed to be an orthogonal mode transition. The remaining PPA sweep under component 1 does not match the trends in the remainder of the PPA data, but must be real. The solid line gives the rotating vector model for $\alpha = 90°$, $\beta = 16°$ and is centered near the sense-reversing circular polarization of component two, strengthening its possible identification as a core component in this picture. The resulting maximum PPA slope is $\sim 3.5°/\mathrm{deg}$.

Another possibility is that the steep sweep in PPA preceding component 1 is real, and no orthogonal mode transition is present at these longitudes. In this case, the sweep under the main peak can be fit by a rotating vector model, but the PPA data accompanying the remainder of the profile cannot be successfully modelled.

The PPA data presented here are significantly different from the results when the pulsar is in a mode of emission with much greater polarization. In that case the PPA data are *extremely* flat. This suggests that the PPA data presented here are not necessarily geometrical in origin, but are due to competition between modes of emission which are non-orthogonal. For non-orthogonal emission modes, the PPA at a given phase depends on the relative frequencies of occurrence of the two modes. If the relative frequencies of occurrence vary across the pulse, then the observed average PPA will vary accordingly. The significant depolarization of the pulsar emission in this emission mode supports this model. The fact that the (presumed) "orthogonal" mode transition preceding the main component does not appear to be completely orthogonal also suggests this interpretation. Similar frequencies of occurrence are, however, required at all radio frequencies to explain the similarity of the 820-MHz and 575-MHz PPA data.

4.3   Shallow PPA Slopes

Xilouris *et al.* (1998) noted that the maximum slopes of the rotating vector models for millisecond pulsars were, on average, significantly flatter than those seen in slow pulsars. The two distributions differ significantly. The observations presented here also indicate that millisecond pulsars have shallow slopes, as can be seen in Table 4.1. The slopes derived here, along with those quoted by Xilouris *et al.* (1998) are listed in columns 4 and 5. The details differ, but the essential flatness of the PPA data remains the same. The distributions of slopes for the populations of normal pulsars and millisecond pulsars are shown in Figure 4.20. These are reproduced from Xilouris
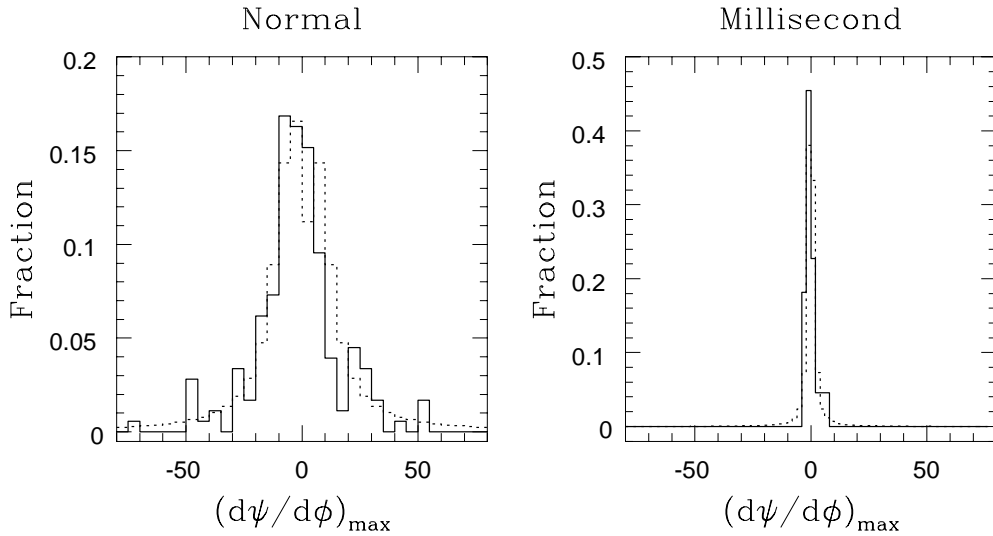
Fig. 4.20.— The distributions of maximum PPA slopes, $(d\psi/d\phi)_{max}$ are displayed. The fraction of pulsars is plotted against slope for both the normal and the millisecond pulsars. The solid-line histograms represent the data, taken from Xilouris *et al.* (1998). The dotted lines result from the simple simulation discussed in the text.

et al. (1998).[1]

Several possible explanations for the flatness of the millisecond pulsar PPA slopes have been discussed. All rely on deviations of the magnetic field from a dipolar structure. In one, special magnetic field geometries created during mass accretion and spin-up are invoked (Chen & Ruderman 1993a). The distorted field can influence the polarization and flatten the PPA curve. Higher order magnetic multipoles near the surface could have a similar effect. For emission near the light cylinder (or at least a polarization limiting radius near the light cylinder), Barnard (1986) has shown that the sweep-back of magnetic fields becomes important, resulting in a flattening of the PPA curve, and its shift to earlier phase. If the absolute emission radius is similar for slow and millisecond pulsars, then this is a tempting interpretation.

These relatively complex explanations are, however, essentially unnecessary. The maximum slope of a simple rotating vector model curve depends on the geometry of

---

[1]It should be noted that the observed PPA slope is a lower limit to the value of the maximum slope. For cases in which the symmetry center is placed in a region of little or no emission, the data constrain the rotating vector model only in the wings, where the curves are flatter. This can result in significantly larger slopes than the data immediately suggest.

the system, as is evident in equation 1.5. For a given inclination angle α, the flattest slopes $(d\psi/d\phi)_{max}$ occur for large impact parameters β. The size of the polar cap ρ is expected to scale with the pulsar rotational period P as $\rho \propto P^{-1/2}$. Since the maximum possible value of impact parameter β for which the pulsar will be visible is ρ, β_{max} must also scale as $P^{-1/2}$. Thus for millisecond pulsars, we expect that the population of visible pulsars will include objects with larger impact parameter β than is true for the population of slow pulsars. This simple fact can, to a large degree, explain the flat slopes of the PPA curves of millisecond pulsars.

With this in mind, we explored the expected observed distribution of slopes for a population of pulsars with random inclinations and impact parameters. For a given period, the maximum impact parameter was set to $\beta_{max} = 6°P^{-1/2}$, comparable to the size of the outer cone of emission in Rankin's model (Rankin 1993). For each of 21 values for the inclination angle α between 0 and 90°, the slope $(d\psi/d\phi)_{max}$ was calculated for 401 values of β from $-\beta_{max}$ to $+\beta_{max}$ (with a slight offset to avoid $\beta = 0$). The resulting distribution of PPA slopes was then normalized to have a cumulative value of one (1).

The above distribution was calculated for 16 different pulsar periods, uniformly distributed in $\log(period)$ between 3 seconds and 0.1 seconds. In order to determine the distribution of PPA slopes for normal (slow) pulsars, these were then combined according to the relative frequency of occurrence of each pulsar period, as determined by inspection of the distribution of pulsar periods from the Princeton Pulsar Catalog (Taylor, *et al.* 1995). Similarly, the millisecond pulsar distribution was determined by an appropriate combination of the distributions for periods of 30, 10, 3, and 1 millisecond.

Figure 4.20 displays the resulting PPA slope distributions. The solid histogram is for the data at 1410 MHz, taken from Xilouris *et al.* (1998). The dashed histogram is a result of the simulation discussed above. Clearly, even this crude simulation recovers many features of the observed distribution. A simple geometric model can explain the data. No unusual magnetic field configurations are required.

The simulation does, however, ignore the difficulties of the fact that the width relationships following $P^{-1/2}$ fail to explain the component widths of millisecond pulsars (cf. Section 4.4).

4.4   Characteristics of Pulse Profiles

The millisecond pulsar polarization profiles discussed here all have several compo-
nents. Most of the objects cannot be classified using the standard methods applica-
ble to slow pulsars. Exceptions to this classification scheme exist even among long-
period objects, but convincing identifications of core and cone pulse components are
rare among the short-period pulsars. Conal components originating from two active
magnetic poles cannot be easily distinguished, due to the large angular extent of the
open-field region above each pole. In addition, components which might otherwise be
considered core components frequently have relatively flat spectra, and flat-spectrum
components are not necessarily located near the center of the pulse profile.

Among slow pulsars, pulsars with dominant core radiation can be distinguished
on the basis of their values of the accelerating potential B/P^2, or on Beskin's Q
parameter, which discriminates between modes of emission in their model (Rankin
1990, Beskin, Gurevich & Istomin 1988) Based on these criteria, virtually all mil-
lisecond pulsars should be dominated by core emission. Most pulse components are,
however, narrower than is predicted for core components using the $P^{-1/2}$ scaling law.
This strongly suggests the possibility that the emission does not fill the open field
line region for short-period pulsars. Intriguingly, the component separations can be
reconciled with the expected conal component separations (appropriately scaled) for
several objects. Little is known about the relationship between the widths of conal
components and pulse period, but the similarity in pulse profile morphology for all
periods suggests that this quantity scales with the conal component separation.

The component separations of millisecond pulsars change very little with radio
frequency (cf. Table 3.1). The same is often true of the pulse widths. This indicates
that the emission region is very compact. The radiation for all frequencies originates
within a narrow range of altitude so that the opening angle of the magnetic field is
the same for all. Very little variation in emission altitude is possible if the radiation
fills the open field lines. This is consistent with the $\pm$ 2 km emission radius for PSR
B1937+21 (Cordes & Stinebring 1984).

The components seen in radio pulse profiles correspond to elementary beams of
emission within the pulsar magnetosphere. Charged particles moving along the open
magnetic field lines determine the current distribution within the magnetosphere (cf.
Section 1.6). The motion of these particles may be perturbed by a plasma instability
or population inversion leading to radio emission (cf. Section 1.7). Elementary beams
of angular size $1/\gamma$ are anticipated, where γ is the relativistic Lorentz factor for the
charges responsible for the emission. The divergence of open field lines in millisecond
pulsars implies that the overlapping of these elementary beams may be reduced for

these objects, particularly if the characteristic beam size is independent of spin period. Structure that is seen in their pulse profiles may therefore be hidden in observations of slow pulsars, as several components may be buried within a single observable structure.

Kramer *et al.* (1998) found that the frequency evolution of the pulse profiles was correlated with the mass of any companion star. This indicates that the evolutionary history has a significant impact on the magnetospheric configuration for these objects. Chen & Ruderman (1993a) propose a concrete example of such evolutionary effects, and suggest that the profile of PSR B1937+21 may have formed in this way. A comparison of this object with the Crab pulsar, however, suggests that its profile, along with that of PSR B1821−24, may be the result of radio emission from the outer-gap region of the magnetosphere. In at least some models (Chen & Ruderman 1993b), the strength of the magnetic field at a given pulse period controls outer-gap emission, and the emission processes in these objects are expected to be similar to those of the Crab pulsar.

4.5 Frequency Dependence of Polarization

The results of Chapter 3 lead to the immediate conclusion that the polarization properties of millisecond pulsars are not strongly dependent on frequency. Figure 4.21 displays the average linear polarization across the pulse, using the data presented in Table 3.3. No strong depolarization with frequency occurs, in contrast to the results for normal pulsars, many of which show significant depolarization at 1.4 GHz (Manchester, Taylor & Huguenin 1973, Morris *et al.* 1981, Morris, Graham & Sieber 1981), relative to observations at lower frequencies.

The lack of depolarization with increasing radio frequency is consistent with the fact that Xilouris *et al.* (1998) found that millisecond pulsars were more highly polarized than normal pulsars at 1410 MHz. The depolarization index is correlated with the accelerating potential $\Delta\Phi \propto B/P^2$ (Xilouris *et al.* 1995). Xilouris *et al.* (1998) note that millisecond pulsars with "abnormal" frequency development tend to have a slightly higher accelerating potential, $\Delta\Phi \propto B/P^2$, as do young core-single pulsars. These latter objects have moderate linear and circular polarization, similar to that seen here. If the voltage $\Delta\Phi$ controls the emission properties, these objects may be related in some way. The two sets of objects also both have $Q > 1$, where Q is a parameter which distinguishes between propagation modes in pulsar magnetospheres (Beskin, Gurevich & Istomin 1988)

McKinnon suggests that the increasing depolarization of pulsars with radio frequency is due to the superposition of orthogonal modes of emission in a birefringent
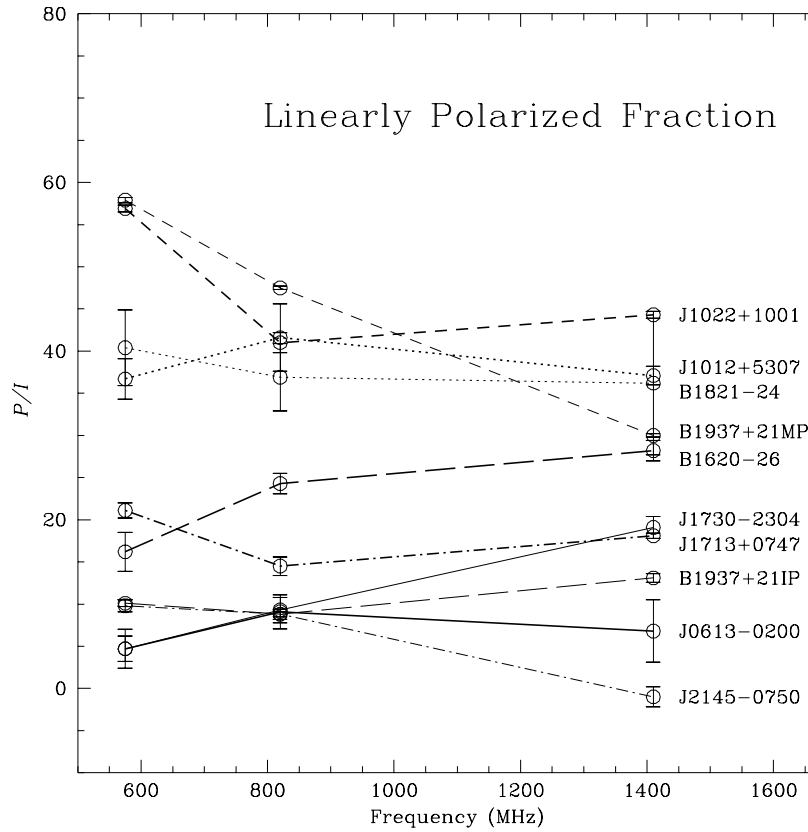
Fig. 4.21.— The fraction of linearly polarized radiation (%), averaged across the pulse, is displayed as a function of frequency for 10 millisecond pulsars. The 1-σ error bars are based on the off-pulse *rms*, and do not include systematic errors, such as those due to incorrect calibration.

medium. The depolarization depends on the relative frequencies of occurrence of the competing modes. Large depolarization rates result when the two modes have similar frequencies of occurrence. This would then suggest that one mode dominates for millisecond pulsars.

Geometric arguments (Morris, Graham & Sieber 1981, Xilouris *et al.* 1995) relate the polarization state of the radio emission to the size of the magnetosphere. Beams of curvature radiation are assumed in this model. Dipolar field lines diverge more for short-period objects, and it is these field lines which control the motion of the charged particles. The increased divergence at short spin periods could result in less overlapping of elementary beams of emission, as noted in Section 4.4, and can result in a larger fraction of linear polarization than is seen in long-period objects. Xilouris *et al.* (1998) reject this argument because it cannot explain the shallow PPA slopes of millisecond pulsars, but we have seen in Section 4.3 that these are also explained by the divergence of the dipolar field lines.

Relative to the pulse peak, the location of orthogonal mode transitions is relatively constant with radio frequency for pulsars B1620−26, J1713+0747 and J2145−0750 (cf. Figures 3.11, 3.14, 3.28). The longitude extent of the orthogonal mode may, however, increase slightly with increasing frequency for PSR J1713+0747. The approximate frequency-independence of these transitions means that the relative frequencies of occurrence of the two orthogonal modes must remain more or less constant with radio frequency. Attributing the complex PPA curve of PSR J2145−0750 to competition between non-orthogonal modes leads to the same conclusion (cf. Section 4.2.9). This can be difficult in models where the orthogonal modes are attributed to propagation effects.

4.6   Moding Behaviour

A number of the pulsars studied here exhibit long-term variations in either the intensity or polarization profiles. This is somewhat surprising in light of the relative constancy of the polarization properties with frequency. This 'moding' behaviour differs from that observed in slow pulsars, in that it occurs on longer time scales, and the transition between modes may be less abrupt.

Of the nine pulsars for which we present multi-frequency data, 3 display long-term variations in the intensity profile (PSRs J1022+1001, B1821−24 and J2145−0750), while at least 5 (PSRs J1012+5307, J1022+1001, J1713+0747, B1821−24 and J2145−0750) exhibit temporal polarization variations at one frequency or another. In addition, comparison of our polarization results at 1410 MHz (including the four pulsars for which we have only 1410-MHz data) with those of Xilouris *et al.* (1998) reveals possible polarization variations for 5 more pulsars (PSRs J0613−0200, J1518+4904, B1620−26, J1640+2224 and J1643−1224). Those authors further note polarization variations for PSRs J0751+1807, J1730−2304, B1855+09 and B1953+29, and profile variations for PSR J1730−2304, and possibly PSR B1953+29. We exclude the variations of the eclipsing pulsar PSR J1744−24A from further consideration, since its polarization properties are a function of orbital phase. These properties are summarized in Table 4.1. Of the thirteen objects in our data set, 3 exhibit temporal total intensity profile variations, while 7-12 vary in their polarization properties. Of the 27 objects in the combined data set, the intensity profiles vary on long time scales for 4-5 pulsars, and the polarization properties change for 9-14 objects.

The average pulse profiles of slow pulsars typically stabilize after a few thousand pulse periods (Helfand, Manchester & Taylor 1975). These stabilization time scales are themselves stable on 20-year time scales (Rathnasree & Rankin 1995). For most slow pulsars, the average profile remains stable. Blaskiewicz (1991) found shape vari-

ations in only 2 of 14 pulsars, while secular changes in the profile of the binary pulsar PSR B1913+16 are attributed to the effects of precession (Weisberg *et al.* 1989). Dramatic intensity mode changes were first reported in the slow pulsar B1237+25 (Backer 1970), and have been identified in several other slow pulsars. These can be accompanied by changes in the polarization properties of the pulsar as well (Bartel *et al.* 1982). Rankin (1986) discussed profile changes in 9 slow pulsars, and sub-pulse drift-mode changes in two others, concluding that mode changing is associated with complex emission profiles, at least in part because the phenomenon is easiest to identify in these cases. At that time, it was unclear whether only a few pulsars exhibited the phenomenon, or if it was simply more readily identifiable in certain objects. Recent polarization observations of 98 pulsars at 1400 MHz were carefully compared by the authors to previous observations when possible (Weisberg *et al.* 1998). This was possible for approximately 60 objects, of which 7 are known to exhibit mode changing at some frequency. Possible profile differences, not obviously attributable to SNR or resolution considerations, were discovered in two pulsars. In one of these, PSR B2020+28, temporal variations in both the intensity and polarization profiles are seen on time scales of days or months, although it is possible that their short daily integration times (2-4 min)[2] do not allow the profile sufficient time to stabilize. Cordes *et al.* (1978) found that on a given day, stable profiles resulted in about 300 pulse periods, but variations between daily averages were present. In addition, the polarization properties of this object exhibited slow variations on a timescale of weeks (Cordes *et al.* 1978). Possible polarization variations were seen in another 12 objects. The polarization differences between the published profiles (which do not have uniform resolution or SNR) are fairly significant in 6 objects, although proper calibration is an issue. Thus, 7-9 of the 60 pulsars exhibit profile variations. Polarization variations may be seen in 5-10 objects, although they are generally subtle.

Intensity variations may occur with similar frequency in the two sets of objects. Temporal changes in the polarization properties are apparently more prevalent in the millisecond pulsar population, however. Profile variations are most easily identifiable in profiles with multiple components. The profiles of millisecond pulsars typically satisfy this criterion.

The intensity profile mode changes in slow pulsars are typically abrupt, and last tens to thousands of pulse periods. PSR B2020+28 is an exception, showing long-term variations in its profile and polarization, as noted above. Another possible example of similar behaviour in the population of slow pulsars is PSR B0355+54.

---

[2]This corresponds to fewer than 1000 pulse periods.

Morris *et al.* (1980) report observations of a single occurrence of a mode change in this object in which the profile apparently changed gradually over ∼ 1000 pulse periods, and remained in the new state for at least 3600 periods. The temporal profile changes observed in the millisecond pulsars occur on much longer time scales. The intensity profile changes of PSR J1022+1001 may be relatively continuous (Camilo 1995), indicating that they are not necessarily as abrupt and distinct as those observed in classic moding behaviour. This may indicate a long-term instability in the emission beam, rather than a switch between a few stable configurations of current in the magnetosphere. The profiles of millisecond pulsars have not been observed on short time scales. The presence of abrupt profile changes lasting 10-1000 periods, analogous to those in slow pulsars, can be neither confirmed nor excluded.

Rathnasree and Rankin (1995) find that the stabilization rate of pulse profiles correlates with beam size ρ. Pulse profiles converge to a stable average faster for objects with larger beam size ρ. This correlation would indicate that we might have expected minimal profile variations in the class of millisecond pulsars, whose open field line region is significantly larger.

The changes in shape of the intensity profiles have particularly disturbing implications for the use of these objects in millisecond pulsar timing programs. These rely on the presence of a stable average profile in order to determine the precise arrival time of each pulse. The effects of the intensity moding of PSR B1821−24 at 1400 MHz are clearly visible in timing data from Green Bank.

4.7   Polarization Summary

Multi-frequency polarimetry observations with high time resolution have been presented for several millisecond pulsars. The polarization position angle (PPA) data, along with information about the total intensity profiles and binary companions, were used to place constraints on the magnetic inclination and observer's location relative to the emission beam.

The polarization properties of the millisecond pulsars are remarkably constant with radio frequency. Little depolarization is observed, in contrast to the observations of slower pulsars. The PPA curves are consistent across a modest range of radio frequency, indicating a probable geometric origin. Orthogonal modes are present in these data, similar to those seen in normal pulsars.

The maximum slopes of the PPA data are much smaller than those for normal, slower pulsars. Unusual configurations of the magnetic field have been suggested as a possible explanation. Here we demonstrated that by scaling the open field line region with the inverse square-root of the period, we can reproduce the characteristics of the observed distributions. Simple geometric considerations can explain this effect.

The components of millisecond pulsars are unusually narrow, and millisecond pulsar intensity profiles are not easily classified according to the slow-pulsar categories. The emission may not fill the open field line region. Outer-gap emission may play a role in a few objects.

Long-term variations are seen in the intensity profiles and polarization properties of millisecond pulsars. The mode changes of slow pulsars typically occur on much shorter time scales. The intensity mode changes observed here have a significant impact on pulsar timing programs for at least one object.